Desalination and Water Treatment
www.deswater.com

doi: 10.5004/dwt.2021.26752

217 (2021) 391–410
March

Methylene blue adsorption from aqueous solution by functionalized perlites: an experimental and computational chemistry study

Eda Gökırmak Söğüt[a,*], Erdem Ergan[a], Necla Çalışkan Kılıç[b], Hakan Dönmez[b], Esvet Akbaş[b]

[a]*Van Security Vocational School, Van Yüzüncü Yıl University, 65080 Van, Turkey, emails: edagokirmak@hotmail.com (E. Gökırmak Söğüt), erdemergan@yyu.edu.tr (E. Ergan)*
[b]*Department of Chemistry, Van Yüzüncü Yıl University, 65080 Van, Turkey, Tel. +904322251024; emails: ncaliskan7@hotmail.com (N. Çalışkan Kılıç), hakan_donmez_65@hotmail.com (H. Dönmez), esvetakbas@yyu.edu.tr (E. Akbaş)*

Received 18 April 2020; Accepted 1 November 2020

ABSTRACT

In this study, 3-aminopropyltrimethoxy-silane (3-APTMS) and 3-mercaptopropyltrimethoxy-silane (3-MPTMS) were used to functionalize perlite in order to increase the adsorption capacity of methylene blue (MB). These materials were characterized by X-ray diffraction, X-ray fluorescence, Fourier transform infrared spectroscopy, scanning electron microscopy, and thermal (thermogravimetry/differential thermal analysis) analyzes. The performance of perlite and functionalized derivatives was tested by adsorption of MB in a batch system under a variable pH (2–11) and initial MB concentration (10–60 mg L^{-1}). Nonlinear and linear Langmuir, Freundlich, Dubinin–Radushkevich (D–R), and Sips adsorption equations were applied to define equilibrium isotherms. The maximum dye sorption was found to be at a pH of 11.0 (96.44% for P_A, 96.51% for P_{APTMS}, and 96.73% for P_{MPTMS}). The adsorption capacity for the dye was found to be 4.9445, 5.2014, and 5.3112 mg g^{-1} for P_A, P_{APTMS}, and P_{MPTMS}, respectively, at 298 K. The adsorption kinetics was best described by the pseudo-second-order model. The obtained results confirm that amino and mercapto functional groups have positive effects on the adsorption of methylene blue by the adsorbents used in this work. Quantum chemical analysis supported better adsorption of methylene blue dye on amine and mercapto-functionalized perlite surfaces than the unmodified surface and the most suitable site for MB adsorption was suggested by Fukui function analysis.

Keywords: 3-aminopropyltrimethoxy-silane; 3-mercaptopropyltrimethoxy-silane; Perlite; Methylene blue; Adsorption characteristics

1. Introduction

Perlite material is an igneous rock rich in silica and 2%–5% of combined water, it is widely occurring amorphous rock formed by cooling of volcanic eruption. In the literature, it is considered an aluminosilicate composed mainly of silica (SiO_2 form) and aluminum (Al_2O_3 form) [1]. Due to its high porosity, ease of use, negligible toxicity, cheap price these along with its chemical and thermal resistance, the applicability of this material will be significant [2]. Perlite has effective adsorptive properties because it contains more than 70% of silica [3]. When heated to a temperature above 870°C, its volume can be expanded up to 20 times its initial volume [4]. The adsorption capacity of perlite depends on the presence of silanols formed by the silicon atoms on the surface of the material [1,5]. Silicon atoms with hydroxyl groups on the surface of perlite tend to sustain their tetrahedral coordination [6]. By adding monovalent hydroxyl groups, they complete their coordination at room

* Corresponding author.

temperature and form silanol groups. Theoretically, it is possible to propose a model containing two or three hydroxyl groups which give silanediol and silanetriol groups of a silicon atom. However, it is impossible for silanetriol groups exist on the silica surface. By incorporating organic functional groups into the material it is possible to improve the physico-chemical properties of aluminosilicates and to increase their application potential [1]. Silylation is the technique of organically functionalized silica surfaces by replacing the acidic hydrogens with hydrophobic alkyl silyl groups [7]. The common reagents used for the silylation are organosilanes [8]. Organic functional groups are added to the silica surface in one of two ways: (1) by post-synthesis reactions (post-synthesis grafting) or (2) by direct synthesis process (co-condensation of silica with organoalkoxysilanes) [9]. Many studies have been carried out on heavy metal removal, in which grafted clays bearing chelating groups or silica-based hybrid materials are used as adsorbents. However, research on the adsorption of dyes by organically modified aluminosilicates is not common [10]. Synthetic dyes are used more in industry than natural dyes because of their low cost production, stability, and variety of colors. Therefore, the removal of industrial wastes containing dyes is one of the most important objectives in environmental research. There are more than 100,000 kinds of dye which are classified as anionic and cationic and about 7×10^5 tons of dyes are produced each year. The cationic dyes contain protonated amine or sulfur containing groups and have a net positive charge [11–13]. Methylene blue (MB) which is a cationic dye is the most commonly used for dying materials, coloring paper, and so on. It is also used as the determination of surface properties, an oxidation–reduction indicator, pesticide industries, antiseptic, and for other medicine purposes. Although the MB is not regarded as a very toxic dye, it can have various harmful effects on human being and animals [14–16]. For this reason, waste containing methylene blue should be removed. Some methods such as chemical precipitation [17], ion-exchange [18], adsorption [19], membrane technologies [20], and photocatalysis [21,22] are used in the removal process. Among these methods, the adsorption method is particularly attractive due to its high removal efficiency, simplicity of design, and ease of use [23].

In recent years, computational chemistry using quantum chemical principles is used to explain the applicability, direction, and prediction of chemical reactions. In pharmaceutical chemistry (in drug design), corrosion (in the study of inhibitors and in the design of new corrosion inhibitors, etc.) is clearly used, however, the adsorption of contaminants from the aqueous solution has not been widely used [24].

In this study, perlite was functionalized with 3-MPTMS and 3-APTMS providing a hybrid organic–inorganic structure. These modified products normally contain an amine (–NH) or thiol group (–SH) which removes impurities by binding the negative charge to metal ions or dye molecules. Perlite and modified perlite samples were characterized and their adsorptive properties were determined. Batch tests were used to investigate the adsorption capacity of methylene blue. In addition, computational chemistry was applied to complete the experimental data in correlating the ease of adsorption with calculated quantum chemical descriptors and to explain the methylene blue adsorption mechanism on these adsorbents [25].

2. Materials and methods

2.1. Materials

The perlite sample was obtained from Erciş/Van deposit in Turkey. Chemicals such as HCl, NaOH, $AgNO_3$, and dry toluene were obtained from Merck (Darmstadt, Germany). In addition, (3-mercaptopropyl) trimethoxysilane and (3-aminopropyl) trimethoxysilane used for modification were purchased from Sigma-Aldrich (St. Louis, USA).

2.2. Purification of perlite

Perlite was treated before using in the experiments as follows: 15 mL of 2 M HCl acid solution was added to 1 g of perlite sample and mixed at approximately 105°C for 4 h. The perlite dispersion was centrifuged and washed repeatedly until it was free of Cl^-. This process was tested using $AgNO_3$ [26]. The purified perlite was dried at 150°C for 24 h and then powdered in porcelain mortar. The adsorbent was labeled as P_A.

2.3. Modification of perlite with organosilanes

Organosilane-modified perlite samples were prepared according to the following procedures: 4 mL of organosilane was dissolved in 50 mL of dry toluene. Then, 1 g of perlite powder was added to this mixture, and the suspension was refluxed for 20 h at 120°C under continuous stirring (400 rpm). The solid phase was filtered and washed several times with dry toluene to remove excess organosilane and dried overnight at 90°C. The same method was repeated for both organosilane (3-aminopropyltrimethoxy-silane and 3-mercaptopropyltrimethoxy-silane) groups [26]. The final products were labeled as P_{APTMS} and P_{MPTMS}.

2.4. Adsorbate

Methylene blue (C16H18N3SCl) with a molecular weight of 319.852 g was obtained from Merck (Darmstadt, Germany) The dye structure is presented in Fig. 1. The initial concentrations were prepared by diluting 1,000 mg L^{-1} stock solution with pure distilled water.

2.5. Sample characterization

Chemical analysis of the P_A, P_{APTMS}, and P_{MPTMS} materials was made using the Philips 2400 X-ray fluorescence (XRF) instrument. The specific surface area of the adsorbents was determined using the Brunauer–Emmett–Teller (BET) method (Quantachrome Nova 2200E surface area and pore size analyzer). The pore diameter was determined by the Barrett–Joyner–Halenda (BJH) adsorption and desorption method based on the conventional Kelvin equation. By means of BJH analysis, pore area, mean pore diameter, and specific pore volume can be determined by using adsorption and desorption techniques. The thermogravimetric (TG), derivative thermogravimetric (DTG), and differential thermal analysis (DTA) data were obtained by

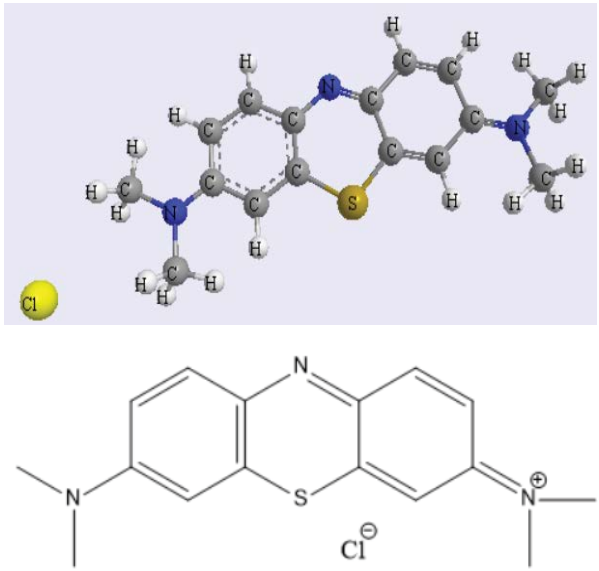

Fig. 1. Chemical structure of methylene blue dye.

a Perkin Elmer (Massachusetts, USA) Diamond instrument with heating from room temperature to 1,099°C temperature at a rate of 20 Kdk^{-1}. X-ray diffraction (XRD) analysis was obtained using a Bruker (Ettlingen, Germany) Axs D8 advance model X-ray diffractometer with Ni-filtered Cu X-ray tube devices at 2°–40°. Fourier transform infrared (FT-IR) analysis was performed using a SHIMADZU (Kyoto, Japan) IRAffinity-1 FT-IR spectrometer with a bandwidth of 400–4,000 cm^{-1}. The morphology of the materials was provided using a scanning electron microscopy (SEM, LEO 440 computer controlled digital).

2.6. Methods

Batch adsorption experiments were carried out in a temperature controlled shaking water bath with a solution of 0.1 g of adsorbent in 10 mL aqueous solution of different concentrations of methylene blue (MB) (10, 20, 30, 45, and 60 mg L^{-1}). A constant agitation speed of 125 rpm was applied at a temperature of 298 K. The contact time of 90 min was found to be sufficient to ensure the equilibrium of adsorption. Upon reaching the determined contact time, the sample were centrifuged at 5,000 rpm for 5 min to separate the solid phase from the liquid phase. After centrifugation, the supernatants were taken using a micropipette and were analyzed to determine the final concentration of MB using a UV-spectrophotometer (Shimadzu UV-1800, Kyoto, Japan) adjusted to a maximum absorption of 665 nm. The amount of adsorbed dye was calculated according to the following equations [27]:

$$q_e = \frac{\left(C_i - C_e\right)V}{m} \tag{1}$$

$$\%\ \text{Adsorption} = \frac{C_i - C_e}{C_i} \times 100 \tag{2}$$

where q_e is the amount of metal ions adsorbed (mg g^{-1}) at the equilibrium time, V is the volume of the solution (L), m is the weight of the adsorbent (g), and C_i and C_e are the dye solution concentration (mg L^{-1}) at the initial and equilibrium times, respectively.

2.7. Point of zero charge measurements

The zero charge point (pH_{pzc}) is defined as the pH at which the adsorbent surface charge takes zero. That is, the charge of positive surface areas is equal to negative surface areas. The pH_{pzc} was calculated by potentiometric mass titrations. The following method was used to determine the surface charge of the adsorbents:

0.03 M KNO_3 was used to obtain a stable ionic strength in determining pH_{pzc}. For potentiometric titration, 0.1 M HNO_3, 0.1 M, and 1 M KOH standard solutions were used. Three different amounts of perlite were weighed and suspensions were prepared. Then, 0.03 M KNO_3 solution was added. The mixture was stirred at 250 rpm for 24 h. Before titration, 1 M KOH was added to deprotonate surface sites. Titration was started by adding 0.05 mL of the HNO_3 (0.1 M) solution to the continuously stirred solution, and pH was recorded in each addition. This process was repeated for a 0.03 M KNO_3 solution without adsorbent. pH_{pzc} was determined from the intersection of potentiometric curves [28].

2.8. Desorption experiments

HCl was used as a desorbent agent in desorption experiments. Ten milliliters of 0.1 M HCl was added to 0.1 g of dye-loaded adsorbent samples and adjusted to pH = 11.0 with NaOH. The mixture was shaken for 60 min, then filtered and the concentration of dye in the filtrate was determined by UV-spectrophotometer. The percentage of desorbed dye ions was calculated by the following Eq. (3) [29]:

$$\text{Desorption}\left(\%\right) = \left(\frac{C_{\text{Des}}}{C_{\text{Ads}}}\right)100 \tag{3}$$

where C_{Des} and C_{Ads} are, respectively, the desorbed and adsorbed concentration of the dye (mol L^{-1}).

2.9. Adsorption isotherms

Langmuir, Freundlich, Dubinin–Radushkevich, and Sips nonlinear and linear isotherm equations were used to describe the nature of the MB adsorption on the P_A, P_{APTMS}, and P_{MPTMS}. The isotherm parameters were determined from a nonlinear regression analysis using a software program (Origin 8.0). Experimentally determined q_e and C_e values are applied to nonlinear equations of adsorption isotherms. The correlation coefficient (R^2), standard errors (SE) for each parameter (the standard deviation of a distribution of a sample statistic) and chi-square (χ^2) values were used to select the best theoretical isotherm [30,31]. These parameters are determined in the following equations:

$$R^2 = \frac{\sum\left(q_{e,\text{calc}} - \overline{q_{e,\text{exp}}}\right)^2}{\sum\left(q_{e,\text{calc}} - \overline{q_{e,\text{exp}}}\right)^2 + \sum\left(q_{e,\text{calc}} - q_{e,\text{exp}}\right)^2} \tag{4}$$

$$\chi^2 = \sum_{i=1}^{N} \frac{\left(q_{e,\exp} - q_{e,\text{calc}}\right)^2}{q_{e,\text{calc}}} \quad (5)$$

where $q_{e,\exp}$ (mg g^{-1}) is determined from the batch experiment, $q_{e,\text{calc}}$ (mg g^{-1}) is calculated from the isotherm for corresponding $q_{e,\exp}$, and $\overline{q_{e,\exp}}$ is the average of $q_{e,\exp}$. Also N characterizes the number of observations in experimental data. To select the most appropriate isotherm model, it is expected that R^2 is closer to 1; χ^2 and S.E. are close to zero [32]. In addition, linear Langmuir, Freundlich, and Dubinin–Radushkevich (D–R) adsorption isotherms were used to better interpret the equilibrium isotherms and compare them with the results obtained from non-linear Langmuir, Freundlich, Dubinin–Radushkevich, and Sips isotherm equations. The above mentioned linear and non-linear isotherm equations are listed in Table 1.

Langmuir isotherm assumes that adsorption occurs in certain homogeneous sites within the adsorbent [38]. The dimensionless separation factor (R_L) calculated using the Langmuir constant (K_L) is expressed by the following equation:

$$R_L = \frac{1}{1 + K_L C_{\text{ref}}} \quad (6)$$

where C_{ref} is any equilibrium liquid phase concentration of the solute. The value of R_L shows the type of the isotherm to be either unfavorable ($R_L > 1$), linear ($R_L = 1$), favorable ($0 < R_L < 1$), or irreversible ($R_L = 0$) [23,34].

The Freundlich isotherm is an empirical isotherm indicating the surface heterogeneity of the adsorbent. The K_F and n (dimensionless) parameters are Freundlich adsorption isotherm constants that are dependent on temperature, adsorbent, and adsorbed compound. The constants express the magnitude of adsorption capacity and the degree of adsorption representing the adsorption intensity, respectively. $n = 1$, the partition between the two phases is independent of the concentration, $(1/n) < 1$ is normal adsorption, $(1/n) > 1$ is cooperative adsorption. Dubinin–Radushkevich isotherm is often used to describe the adsorption mechanism with a Gaussian energy distribution onto a heterogeneous surface. The constant β gives an idea about the mean free energy E (kJ mol^{-1}) of adsorption and can be computed using the equation in the Table 1. If the energy (E) < 8 kJmol^{-1}, adsorption can be explained with physical interactions. On the other hand, if the energy > 8 kJmol^{-1}, adsorption mechanism can be clear with chemical interactions [23,30].

Sips isotherm is a combination of the Langmuir and Freundlich isotherms and is suitable for describing the adsorption process on heterogeneous surfaces. The Sips isotherm equation is defined by n_S, the dimensionless heterogeneity factor. When the value is 1, the Sips equation is reduced to the Langmuir equation, which indicates that the adsorption process is homogeneous [37].

2.10. Adsorption kinetics

Kinetic parameters were evaluated for the adsorption of MB onto the P_A, P_{APTMS}, and P_{MPTMS} adsorbents using nonlinear and linear equations of pseudo-first-order (PFO), pseudo-second-order (PSO) kinetic models, and intraparticle diffusion and Boyd models. The main characteristics of PFO and PSO kinetics are based on the fact that the adsorption steps (including external and internal diffusion/adsorption) are combined [24]. The intraparticle diffusion model is used to determine the rate limiting step of the sorption kinetics. This model assumes that the adsorption mechanism occurs by diffusion of adsorbate molecules into the pores of the adsorbent material [39]. The Boyd kinetic equation was applied to determine the rate limiting step of the MB adsorption process [40–42]. The kinetic model equations are listed in Table 2.

2.11. Computational chemistry study

The theoretical calculations of all compounds and the adsorption potential are explained using QCCs based on DFT [43]. According to molecular orbital theory; all molecules have highest occupied molecular orbital (HOMO) and lowest unoccupied molecular orbital (LUMO). Using the HOMO and LUMO energy values of a molecule, the following parameters can be found: ionization potential ($I = -E_{\text{HOMO}}$), electron affinity ($A = -E_{\text{LUMO}}$) electronegativity ($X = I + A/2$), chemical hardness ($\dot{\eta} = I - A/2$), chemical softness ($S = 1/2\dot{\eta}$). In addition, spherical electrophilicity index (ω), transmitted electron fraction index (ΔN), and back donation were calculated according to Karzazi et al. [44–47].

3. Results and discussion

3.1. Materials characterization

The chemical composition of P_A, P_{APTMS}, and P_{MPTMS} was determined by X-ray fluorescence and presented in Table 3.

Table 3 illustrates that the main components of the P_A are silica, 72.83%, and alumina, 11.92%. No significant change was observed in these values after modification. Silica and alumina values were determined as 71.29% and 11.24% for P_{APTMS} and 69.12% and 11.37% for P_{MPTMS}, respectively.

The physical characteristics of the perlite and modified perlite samples are shown in Table 4. Perlite is considered a mesoporous material (20–500 Å pore diameter), with an average pore radius of 19.99 Å and BET specific surface area of 0.994 m^2 g^{-1} [4].

There was a slight decrease in the BET specific surface area of the P_{APTMS} sample (0.835 m^2 g^{-1}), but an increase in micropore volume and pore diameter. The specific surface area of the P_{MPTMS} sample (1.361 m^2 g^{-1}), micropore volume (6.282 E-03 cc g^{-1}), and pore diameter (39.34 Å) were significantly increased.

The X-ray diffractogram shows that Fig. 2, P_A and modified perlites (P_{APTMS} and P_{MPTMS}) are amorphous materials. The broadband in the range of 2θ ~20°–35° indicates the amorphous structure. Amorphous silica and small amounts of opal-CT, quartz, feldspar, montmorillonite, mica, illite, calcite, and kaolinite are detected in the P_A sample. The modification did not change the structure of perlite. Fig. 2 shows that the intensities change while the positions of the peaks are unchanged [48,49].

Table 1
Non-linear and linear equations of the isotherm models

Isotherm	Non-linear equation	Linear equation	Constants	Reference
Langmuir	$q_e = \frac{q_M K_L C_e}{1 + K_L C_e}$	$\frac{1}{q_e} = \frac{1}{K_L q_M} \times \frac{1}{C_e} + \frac{1}{q_M}$	K_L is the Langmuir isotherm constant (L g^{-1}) q_M is the monolayer capacity	[33,34]
Freundlich	$q_e = K_F C_e^{\frac{1}{n}}$	$\log q_e = \log K_F + \frac{1}{n}\log C_e$	K_F is the Freundlich isotherm constant (L g^{-1}) n is the heterogeneity factor in the Freundlich model	[35]
Dubinin–Radushkevich	$q_e = q_M \exp\left(-K_{DR}\varepsilon^2\right)$ $\varepsilon = RT \ln\left(1 + \frac{1}{C_e}\right)$	$\ln q_e = \ln q_M - K_{DR}\varepsilon^2$	q_M is D–R adsorption capacity (mg g^{-1}) K_{DR} is the constant related to adsorption energy (mol^2 kJ^{-2}) ε is the energy of adsorption R is the ideal gas constant (8.314 (J mol^{-1} K^{-1})	[36]
Sips	$q_e = \frac{q_M a_S C_e^{(1/n)}}{1 + a_S C_e^{(1/n)}}$	$\frac{1}{q_e} = \frac{1}{q_M K_S}\left(\frac{1}{C_e}\right)^{(1/n)} + \frac{1}{q_{\max}}$	K_S is the Sips isotherm constant (L g^{-1}) a_S is the Sips isotherm constant (L mg $^{-1}$) n_S is the dimensionless heterogeneity factor	[17,37]

Table 2
Non-linear and linear forms of kinetic models [9,41]

Non-linear equations	Linear equations	Kinetic models	Constants
$q_t = q_e\left[1 - \exp\left(-k_1 t\right)\right]$	$\ln\left(q_e - q_t\right) = \ln q_e - k_1 t$	Pseudo-first-order	k_1 (min^{-1}) is the pseudo-first-order rate constant t (min) is the contact time
$q_t = \frac{k_2 q_e^2 t}{1 + k_2 q_e t}$	$\frac{t}{q_t} = \frac{1}{k_2 q_e^2} + \frac{t}{q_e}$	Pseudo-second-order	k_2 (g mg^{-1} min^{-1}) is the pseudo-second-order rate constant
	$q_t = k_{id}\sqrt{t} + C_i$	Intraparticle diffusion	k_{id} is intraparticle diffusion constant C_i is the intercept value (gives an indication about the thickness of boundary layer)
	$B_t = -0.4977 - \ln\left(1 - F\right)$ $F = \frac{q_t}{q_e}$	Boyd	F is the fractional attainment of equilibrium, equal to q_t/q_e B_t is a mathematical function of F

Table 3
Chemical composition of adsorbents by XRF analysis

P_A		P_{APTMS}		P_{MPTMS}	
SiO_2	72.83	SiO_2	71.29	SiO_2	69.12
Al_2O_3	11.92	Al_2O_3	11.24	Al_2O_3	11.37
K_2O	5.14	K_2O	4.8	K_2O	4.77
Na_2O	2.71	Na_2O	2.77	F	3.38
Fe_2O_3	1.6	F	2.41	Na_2O	2.69
CaO	0.65	Fe_2O_3	1.5	Fe_2O_3	1.5
TiO_2	0.09	CaO	0.63	CaO	0.61
P_2O_5	0.06	TiO_2	0.06	SO_3	0.19
BaO	0.06	Cl	0.05	TiO_2	0.07
MnO	0.05	BaO	0.04	BaO	0.06
Loss on ignition (%)	4.90		5.20		6.25

Table 4
Specific surface area, micro-pore volume, and pore diameter values obtained by BET and BJH methods

Adsorbent	Specific surface area (BET) (m^2 g^{-1})	micro-pore volume (cc g^{-1})	pore diameter (Å)
P_A	0.994	3.701 E-03	19.99
P_{MPTMS}	1.361	6.282 E-03	39.34
P_{APTMS}	0.835	6.106 E-03	35.10

TG-DTA-DTG curves for P_A, P_{APTMS}, and P_{MPTMS} are shown in Figs. 3a–c, respectively.

The TG curves revealed the dehydration/dehydroxylation of perlite and the decomposition of organic modifiers on the surfaces of perlite. From the TG curve of P_A

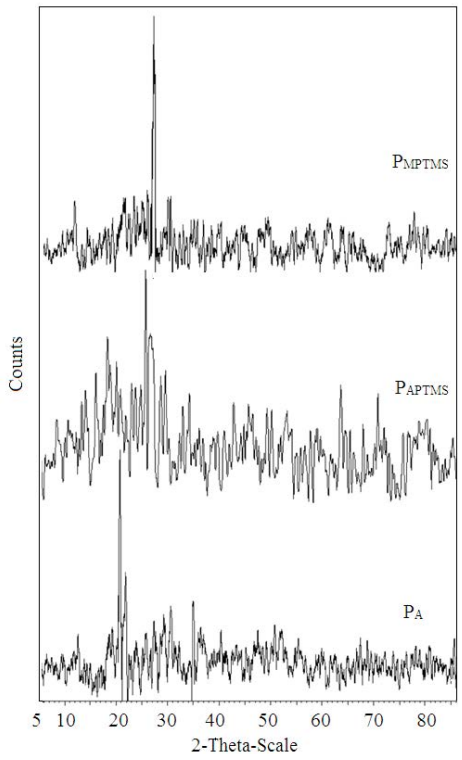

Fig. 2. XRD patterns of P_A, P_{APTMS}, and P_{MPTMS}.

(Fig. 3a), there are three sharp mass losses of 2.1% between 200°C and 300°C, which should be associated with the loss of water consistent. Next, the TG curve shows a gradual decrease in the 300°C–850°C range. Mass loss between 300°C and 850°C was observed to be about 2.3%. Total mass loss is 4.4%. After this temperature, it is observed that the material remains thermally stable to the final analysis temperature (1,099°C). The DTG curve, Fig. 3a, shows peaks around 200°C, 250°C, and 300°C. These peaks depend on the observed weight loss in the range of 200°C–300°C in TG analysis. DTA curve show exothermic peaks at 300°C and 960°C are due to thermal degradation. Similar behavior is observed in modified P_{APTMS} and P_{MPTMS} materials. This is attributed to the removal of water introduced into the structure during the functionalization process being applied [9,50]. In Figs. 3b and c, the functionalized samples show mass losses of up to 200°C resulting from the release of adsorbed water and >500°C is due to the dehydroxylation of the silicate layers. It showed additional weight loss from 200°C to 600°C of loss of silane molecules in the structure. The first DTG peaks around 250°C and 275°C may be attributed to weaker bound silane molecules. At about 570°C, the DTG peak results from strongly bonded silane molecules in the intermediate layer cavity [51].

FT-IR analyzes were performed in the 450–4,000 cm^{-1} band. The main absorption bands for P_A, as depicted in Fig. 4, were found at 3,741; 3,622; 1,643; 1,627; 1,512; 1,060; 783; 644; and 459 cm^{-1}. A strong band at 1,060 cm^{-1} and a

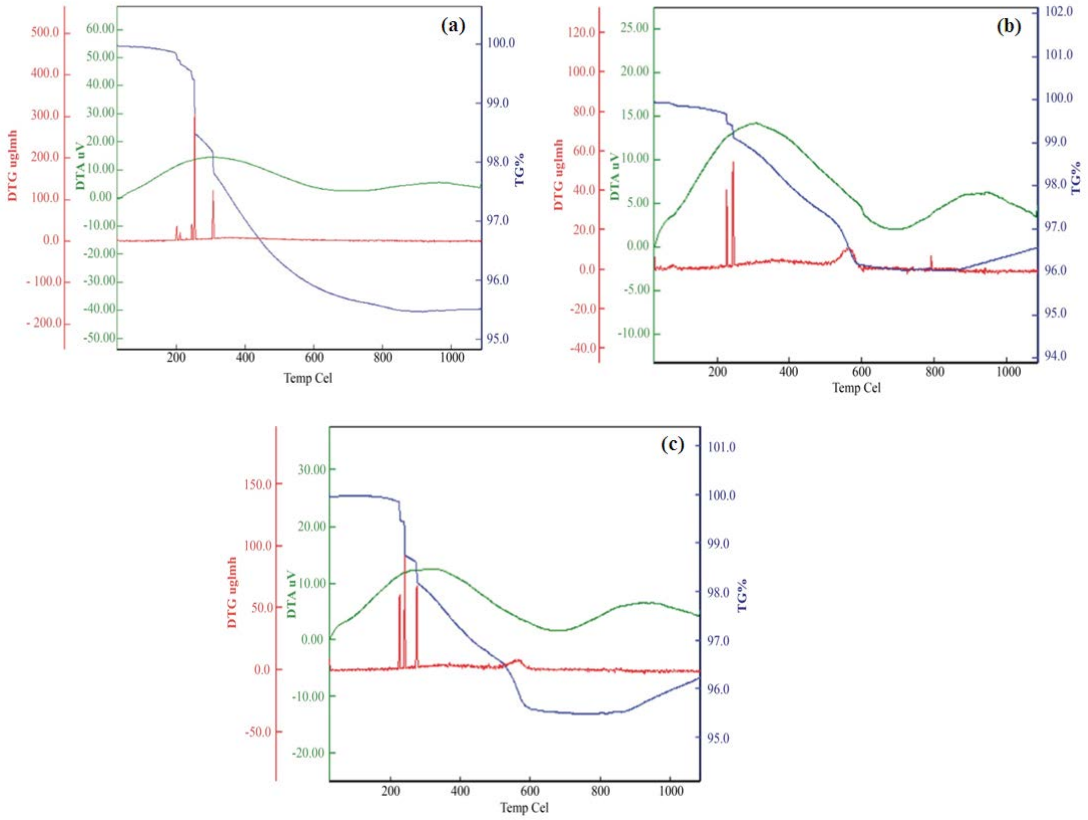

Fig. 3. TG, DTG, and DTA curves of (a) P_A, (b) P_{APTMS}, and (c) P_{MPTMS}.

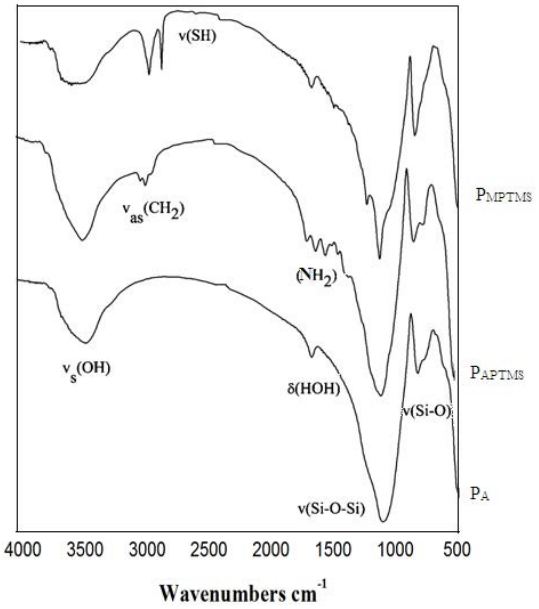

Fig. 4. FTIR spectrum of perlite P_A and functionalized perlite with 3-APTMS and 3-MPTMS.

weaker band at 783 cm^{-1} attributed to Si–O stretching vibrations of Si–O–Si and Si–O–Al, respectively, and there is another strong band at 459 cm^{-1} due to O–Si–O bending [52]. The band at about 3,700 cm^{-1} can be attributed to the surface isolated hydroxyl groups bonded to silicon and the band at 1,643 cm^{-1} is related to the C–O vibration. The adsorption band at 1,627 cm^{-1} is due to deformation vibrations of adsorbed water molecules (δH–O–H) [9]. The range of 3,000–3,800 cm^{-1} band is isolated in different environments and assigned to the stretching vibrations of surface –OH groups [53]. The 3,741 cm^{-1} band is the contribution of free terminal Si–OH groups. The FTIR spectra (Fig. 4) of the modified samples (P_{APTMS} and P_{MPTMS}) showed a strong band at 3,622 cm^{-1} related to the stretching vibration of the structural hydroxyls group (AlAlOH, AlMgOH), typical of montmorillonite [51]. In the P_{MPTMS} sample, the presence of –SH group is demonstrated by the presence of a weak –SH absorption at 2,553 cm^{-1} [54]. The FTIR spectra of the P_{APTMS} exhibit deformation of $–NH_2$ at 1,566 cm^{-1} and CH_2 deformation at 1,485 cm^{-1} [26]. The aliphatic CH_2 groups lead to a doublet at 2,939 and 2,835 cm^{-1}, which is given to asymmetric and symmetric stretching, respectively [51].

The SEM image of perlite shows a substantially smooth and fine porous and glassy structure (Figs. 5a–c). The perlite particles have irregular morphology and have an average range of 1–20 μm as shown in Fig. 5a. Similar structures are also compatible with different perlite samples [55]. The surface of modified perlite, Figs. 5b and c, is enclosed by the aggregates; this shown the modification process of perlite by organosilanes.

3.2. Effect of pH

The solution pH affects the surface charge of the adsorbent and the degree of ionization of the adsorbate [56,57]. The effect of pH on adsorption of MB was studied between 2 and 11. The initial dye (MB) concentration was 30 mg L^{-1}, the adsorption contact time was 90 min. The pH was adjusted by the addition of 0.1 mol L^{-1} NaOH or HCl solutions. The pH_{pzc} of the P_A, P_{APTMS}, and P_{MPTMS} samples were determined to be 2.5, 3.5, and 2.4, respectively; and after the modification of aminosilane, the presence of $–NH_2$ groups changed the surface charge of the P_{APTMS} to the basic character and pH_{pzc} increased [58]. Fig. 6 shows the change in the amount of MB dye adsorbed onto P_A, P_{APTMS}, and P_{MPTMS} with pH.

As can be clearly seen from the graph, with the increase of the adsorption values of pH 4 and 5 for P_A, there was a decrease after. A significant increase in adsorption efficiency is observed for all adsorbents after pH 9. In the adsorption experiments, the pH effect was investigated and the optimum removal was performed at pH 11. Generally, pH can affect various solution factors such as charge, degree of decomposition, or ionization [23]. The removal efficiency is lower at lower pH values. The excess H ion makes the perlite surface positive, which in turn affects the pushing force between the molecules, thereby causing a reduction in dye adsorption. Doğan et al. [59] emphasized that perlite are not zero charge points and show negative zeta potential values in the 3–11 pH range. This negative charge may be due to isomorphic substitutions within the perlite structure of Al^{3+} for Si^{4+}, defects in the crystal lattice, broken particle edges, and structural hydroxyl groups [60].

The higher the pH of the dye solution, the easier the dye cations interact with the negatively charged perlite surfaces [6].

$$–MOH + OH– = –MO– + H_2O \quad (7)$$

$$–MO + Dye^+ = –M – O – Dye \quad (8)$$

As shown in Fig. 6, the amount of methylene blue adsorbed to P_A at pH 4 and 5 is greater than that of the modified perlite samples. The decrease in MB adsorption on modified perlites may be the result of some events, such as an increase in the micro pore volume occurring during the modification and/or the amount of the –SH and –NH groups in the structure being less than the hydroxyl groups. At pH 11, the activity of MB adsorption of perlites is in the order of $P_A < P_{APTMS} < P_{MPTMS}$.

3.3. Adsorption isotherms

The adsorption isotherms of MB onto perlite and modified perlite samples at 298 K temperature were studied. The effect of dye concentration in the range from 10 to 60 mg L^{-1} on the sorption process is shown in Fig. 7. It was determined that the adsorbed amount increased with increasing MB concentration. Also, the effect of adsorbent modification on adsorption is in $P_A < P_{APTMS} < P_{MPTMS}$.

The experimental data were applied to the linear and nonlinear Langmuir, Freundlich, D–R, and sips adsorption models using the equations in Table 1. Figs. 8–10 show adsorption equilibrium isotherms for adsorption of MB onto P_A, P_{APTMS}, and P_{MPTMS} in the system, respectively.

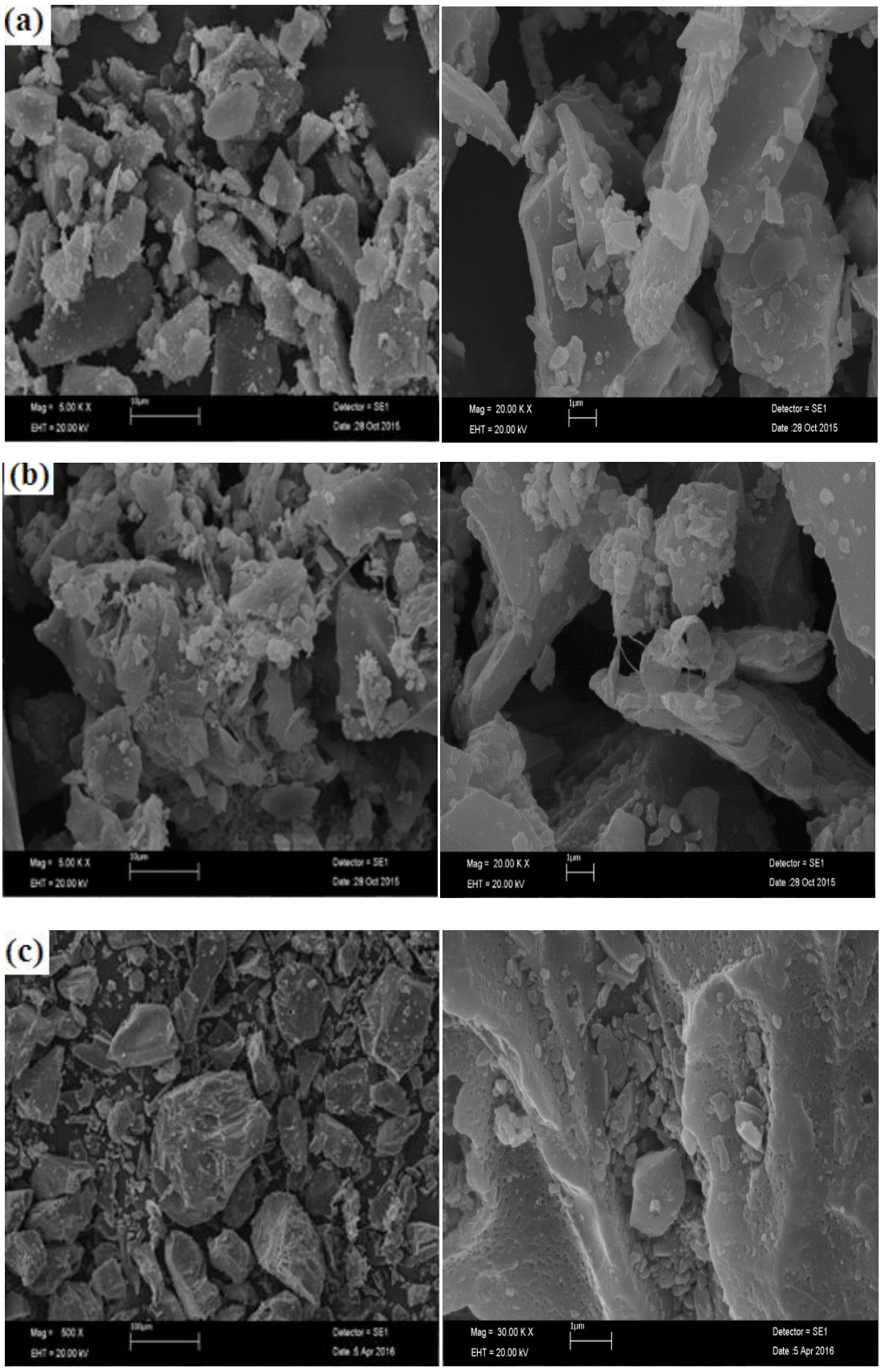

Fig. 5. Micrographies of (a) P_A, (b) P_{APTMS}, and (c) P_{MPTMS}.

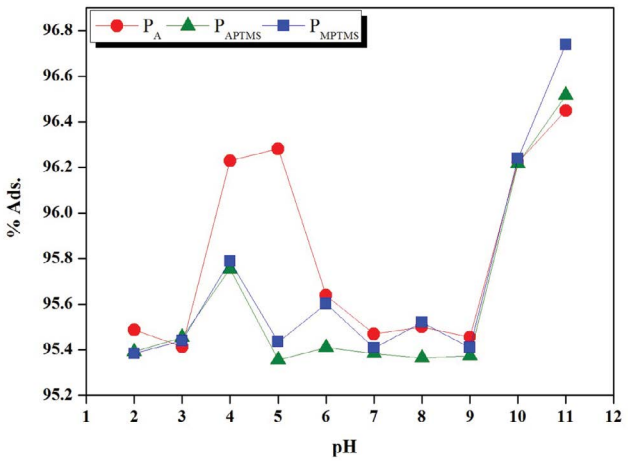

Fig. 6. Effect of pH on removal of MB dye with concentrations of 30 mg L^{-1} on perlite samples (T = 298 K).

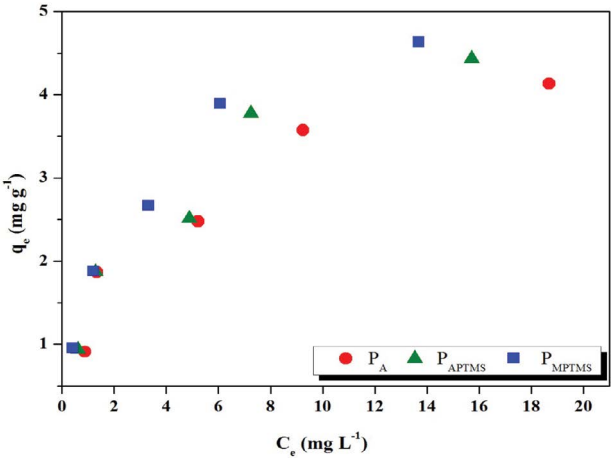

Fig. 7. Equilibrium studies of MB removal by the perlite samples (T = 298 K, pH = 11.0).

The parameter values and correlation coefficients of the linear and non-linear isotherm models for MB adsorption at pH 11.0 are given in Table 5 [30].

The plots of $1/C_e$ vs. $1/q_e$ (Figs. 8a, 9a, and 10a) were used to determine the Langmuir isotherm parameters (K_L and q_m) and the results are given in Table 5. The Langmuir monolayer adsorption capacities (q_m) of MB were determined to be 4.6524, 5.1196, and 5.4470 mg g^{-1} at 298 K for P_A, P_{APTMS}, and P_{MPTMS}, respectively. The R_L values for adsorption of MB on the adsorbent surface are between 0 and 1; this indicates

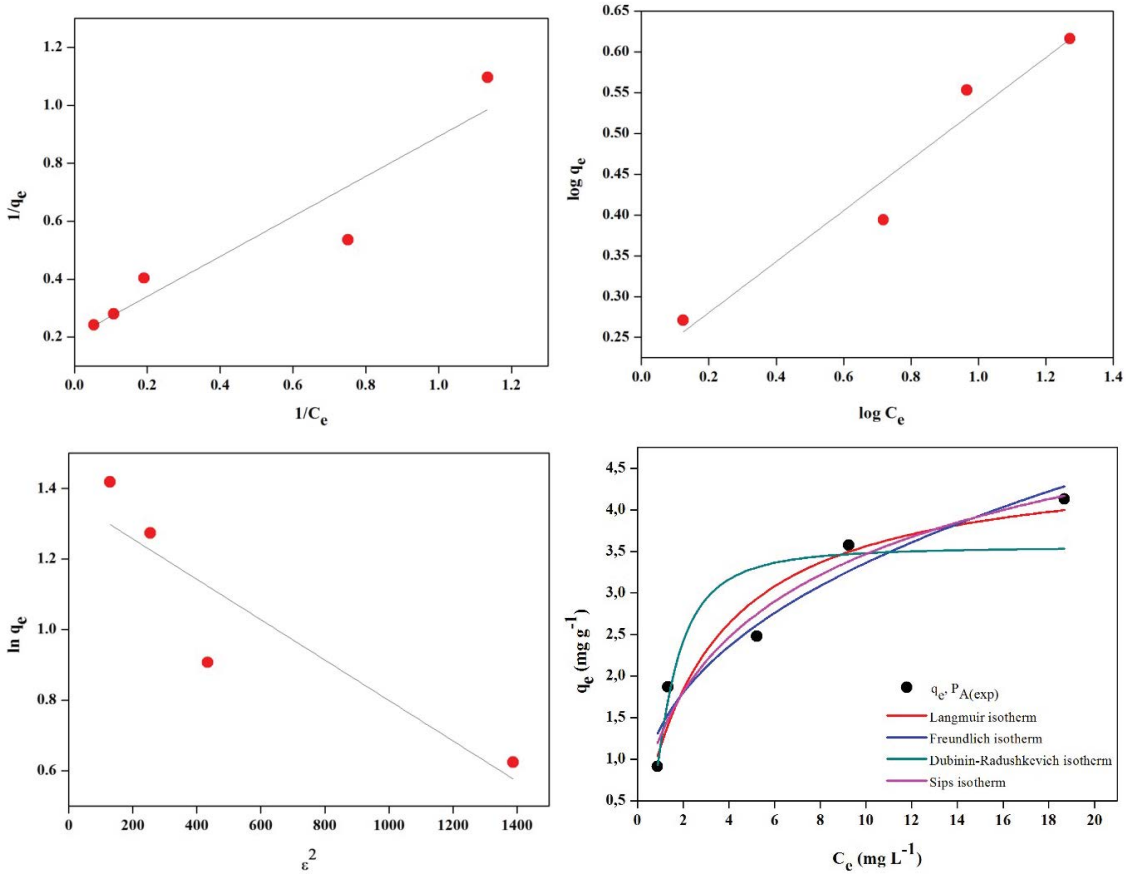

Fig. 8. Equilibrium studies of MB adsorption by the P_A, (a) Langmuir, (b) Freundlich, (c) D–R models, and (d) theoretical treatment of the three models and Sips model (T = 298 K, pH = 11.0).

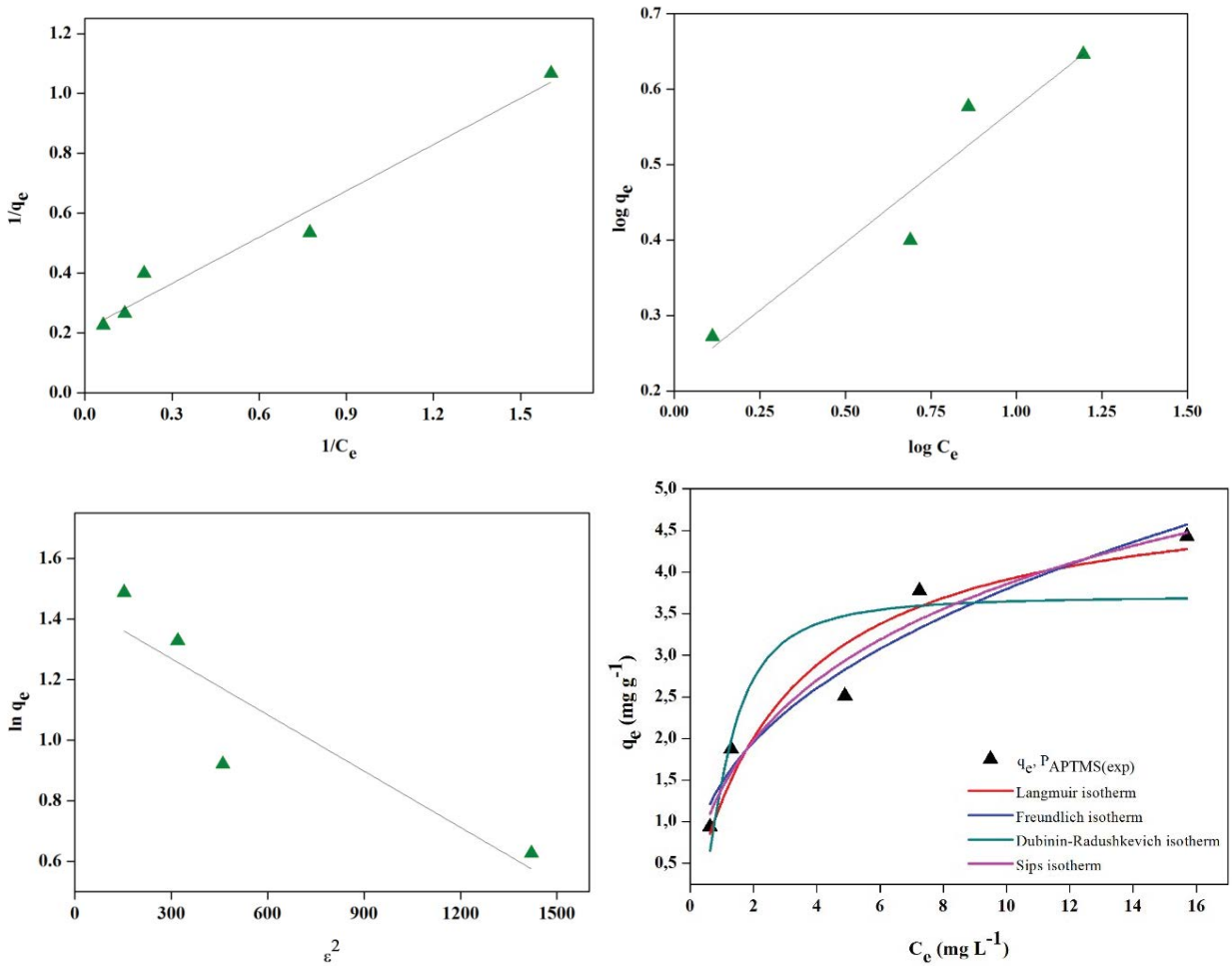

Fig. 9. Equilibrium studies of MB adsorption by the P_{APTMS}, (a) Langmuir, (b) Freundlich, (c) D–R models, and (d) theoretical treatment of the three models and Sips model (T = 298 K, pH = 11.0).

favorable adsorption on the surface of P_A, P_{APTMS}, and P_{MPTMS}. The adsorption coefficients, the K_L value associated with the apparent sorption energy for P_{MPTMS}, are greater than the other adsorbents. Also, χ^2 values are calculated as 0.1527, 0.1959, and 0.0739, respectively, for three adsorbents.

The values of K_F and n were calculated from the plot of $\log q_e$ vs. $\log C_e$ (Figs. 8b, 9b, and 10b) The Freundlich isotherm gives a better fit particularly for MB adsorption from solution (correlation coefficient, R^2 = 0.9187 (P_A), 0.9242 (P_{APTMS}), and 0.9597 (P_{MPTMS}). The $1/n$ value of a good adsorbent is expected to be in the range of 0.4 to 0.9 [61]. Also, χ^2 values are close to zero and R^2 values being close to 1.

The E values were calculated from the D–R equation as 3.7796, 4.1309, and 3.9228 kJ mol^{-1} for adsorption of MB dye onto P_A, P_{APTMS}, and P_{MPTMS}, respectively. Since these values are lower than 8 kJ mol^{-1}, the adsorption of MB onto perlite and modified samples is likely to be physical in nature.

Sips isotherm constants (n_S) from Table 5 confirm the heterogeneous nature of the surfaces of P_A (0.6387), P_{APTMS} (0.6037), and P_{MPTMS} (0.7138). From the non-linear four isotherm models (Figs. 8d, 9d, and 10d), it was determined that the Freundlich model was best suited to experimental data (Table 5). The adsorption capacities of these adsorbents in the system have been compared with some alternative adsorbents reported in the literature (Table 6) [41,48,62–69].

Perlite does not show a distinct superiority compared to other newly developed adsorbents and activated carbon. The comparison of the capacities without considering the cost and possible by-products during the preparation and use of materials does not provide sufficient information. Activated carbon is one of the most popular adsorbents but has some disadvantages. For example, activated carbon leads to greenhouse gas emissions during production (6.6 kg CO_2 kg^{-1}) and requires high energy demand (97 MJ kg^{-1}) [70]. Many newly developed adsorbents are also known to be costly and cause secondary pollution. However, perlite is a natural and economical material.

3.4. Kinetic study

The adsorption capacity of the adsorbents was measured as a function of contact time to establish an optimum time for maximum dye uptake and to evaluate the kinetics of the process (Fig. 11).

Sorption of MB from a solution by the P_A, P_{APTMS}, and P_{MPTMS} at different contact times (1, 5, 10, 20, 30, 45, 60, 75,

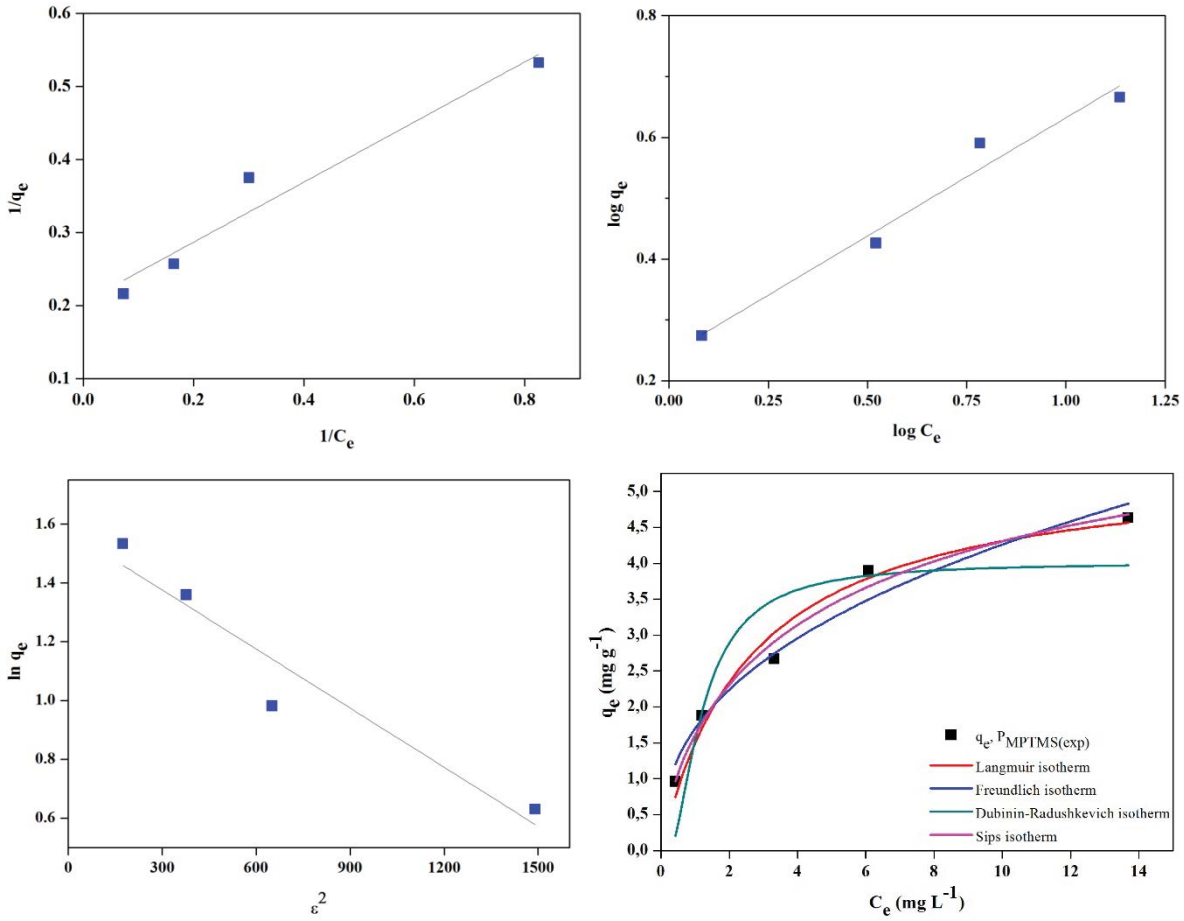

Fig. 10. Equilibrium studies of MB adsorption by the P_{MPTMS}, (a) Langmuir, (b) Freundlich, (c) D–R models, and (d) theoretical treatment of the three models and Sips model (T = 298 K, pH = 11.0).

90, and 120 min) and room temperature (298 K) was investigated and the time required to reach maximum adsorption was determined as 90 min [48]. It was observed that the adsorption of methylene blue for all three adsorbents was rapid at the initial stage of contact time and then slowed gradually. The removal of methylene blue by adsorption on the surface of perlite resulted from the presence of MB^+ cationic form. Adsorption kinetics, such as PFO, PSO, intraparticle diffusion, and Boyd models were investigated to provide a mechanism and useful data about the efficiency of the adsorption process [71]. Fig. 12 shows the graphs of PFO and PSO kinetic models for the removal of MB at 298 K. The determined kinetic parameters of these models are given in Table 7.

When the correlation coefficient values (R^2) were compared, the kinetic data were well-defined by the PSO kinetic model for adsorption of MB. In addition, the calculated adsorption capacities ($q_{e,cal}$) of the PSO kinetic model were determined to be very close to the experimental adsorption capacities ($q_{e,exp}$) [72]. In order to explain the diffusion mechanism and to determine the rate limiting step in the adsorption process kinetic data were analyzed by the intraparticle diffusion and Boyd models [40,73]. In solid–liquid adsorption system, the process is given in the following three steps:

In the first step, the adsorbate molecules are transported to the outer surface of the adsorbent (film diffusion). In the second step, the adsorbate molecules are diffused into an adsorption site via liquid-filled pores (pore diffusion or intraparticle diffusion). In the third step, the adsorbate molecules interact at a site of the adsorbent (internal or external). This step is not considered a rate limiting step because it is relatively faster than the other two steps. Therefore, diffusion steps (film diffusion or pore diffusion) are rate limiting in the adsorption process. Adsorption rate is controlled by film diffusion or intraparticle diffusion or both [40].

The intraparticle diffusion is the plot of the amount sorbed per unit weight of sorbent, q_t (mg g^{-1}) vs. square root of time, $t^{1/2}$, is shown in Fig. 13a (P_A), 13b (P_{APTMS}), and 13c (P_{MPTMS}) for initial MB concentration of 30 mg L^{-1} at 298 K.

Figs. 13a–c show that the adsorption plots are non-linear over the whole time range and can be divided into multi-linear regions which confirm the multi stages of adsorption. The presence of these linear stages reflects the difference in the mass transfer rate of MB adsorption in the initial and the final stages [73].

The first step is attributed to the boundary layer diffusion of adsorbate, the second step describes the intraparticle or pore diffusion step in which the dye moves into the adsorbent particles and adsorbed into the internal regions

Table 5
Parameters of isotherms models for MB removal by P_A, P_{APTMS}, and P_{MPTMS}

Isotherm/ Model		P_A				P_{APTMS}				P_{MPTMS}			
		Linear		Non-linear		Linear		Non-linear		Linear		Non-Linear	
		Value	S.E	Value	S.E.	Value	S.E.	Value	S.E.	Value	S.E.	Value	S.E.
Langmuir	q_M (mg g^{-1})	4.9445	0.0852	4.6524	0.5661	5.2014	0.0420	5.1195	0.7485	5.3112	0.0293	5.4470	0.4561
	K_L	0.3223	0.13814	0.3264	0.1279	0.3929	0.0522	0.3227	0.1437	0.4578	0.0654	0.3782	0.0940
	R_L	0.1343	–	0.1328	–	0.1128	–	0.1341	–	0.0984	–	0.1167	–
	R^2	0.8671	–	0.9088	–	0.8547	–	0.9017	–	0.9518	–	0.9223	–
	X^2	–	–	0.1526	–	–	–	0.1958	–	–	–	0.0739	–
Freundlich	K_F	1.6521	0.0446	1.3772	0.2233	1.6481	0.0614	1.4719	0.2347	1.7529	0.0344	1.6995	0.1759
	$1/n$	0.3128	0.0508	0.3876	0.4543	0.3580	0.0753	0.4115	0.4224	0.3884	0.0465	0.3993	0.3110
	R^2	0.9662	–	0.9187	–	0.9189	–	0.9242	–	0.9720	–	0.9696	–
	X^2	–	–	0.1361	–	–	–	0.1511	–	–	–	0.0888	–
Dubinin–Radushkevcih	q_M (mg g^{-1})	3.9432	0.1358	3.4436	0.3727	4.2874	0.1617	3.7107	0.4541	4.8413	0.1104	4.0093	0.5060
	$K_{D–R}$	0.0572	0.0018	0.0349	0.8601	0.0619	0.0021	0.0293	0.8980	0.0669	0.0041	0.0324	1.0059
	$E_{D–R}$	2.9565	–	3.7796	–	2.8421	–	4.1309	–	2.7338	–	3.9228	–
	R^2	0.8300	–	0.7834	–	0.7184	–	0.7302	–	0.8926	–	0.7438	–
	X^2	–	–	0.3627	–	–	–	0.5378	–	–	–	0.5639	–
Sips	q_M (mg g^{-1})	–	–	7.0922	7.2588	–	–	9.1850	1.3236	–	–	7.1975	2.6453
	a_S	–	–	0.0933	0.3092	–	–	0.0585	0.2636	–	–	0.1747	0.1948
	n_S	–	–	0.6387	0.4356	–	–	0.6037	0.4152	–	–	0.7138	0.2130
	R^2	–	–	0.8977	–	–	–	0.8989	–	–	–	0.9733	–
	X^2	–	–	0.1712	–	–	–	0.2015	–	–	–	0.0586	–

Table 6
Maximum adsorption capacities (q_e) and comparison with other adsorbents

Adsorbent	Modification agent	Dye adsorbed	Maximum adsorption capacity, q_e (mg g^{-1})	Reference
Pal-APTES	APTES	MB	49.48	[48]
		MY	47.03	
Sep-APTES	APTES	MB	60.00	
		MY	59.78	
Activated carbon	Ficus carica Bast	MB	47.62	[62]
Perlite	–	MB	6.65	[63]
		MG	3.87	
		MV	4.98	
Pumice powder (I)	–	MB	0.442	[64]
Pumice powder (II)	–	MB	1.488	
Fly ash	–	MB	5.718	[41]
Magadiite	CTAB-KH550	MB	96.6	[65]
Modified pumice	HCl	MB	15.87	[64]
Graphene oxide	(–SH)	MB	763.30	[66]
	(–NH_2)		676.22	
Activated carbon fiber (ACF)	–	MB	500	
Granular activated carbon (ACG)	–	MB	250	[67]
Activated carbon fiber (ACF)	–	MB	175.44	[68]
Nanoparticles (NPs	NiO	MB	166.67	
	Cu	MB	28.66	[69]
Modified perlite	HCl	MB	4.94	This study
	(–NH_2)	MB	5.20	
	(–SH)	MB	5.31	

MB: methylene blue; MY: metanil yellow; MG: malachite green; MV: methyl violet.

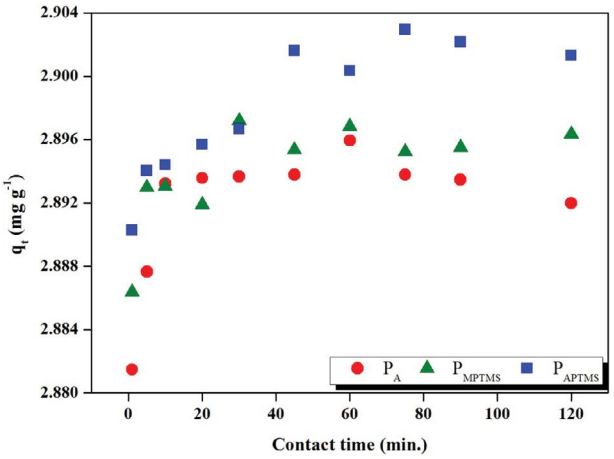

Fig. 11. Effect of contact time on adsorption amount of MB (T = 298 K, pH = 11.0).

of the adsorbents [40], and the third linear region indicated adsorption/desorption equilibrium [23].

If the intraparticle diffusion is the only rate-limiting step, it is essential for the q_t vs. $t^{1/2}$ plots to go through the origin. Moreover, these plots (Figs. 13a–c) not only fitted with a straight line passing through the origin but also with poor linear regression coefficients (R^2) indicating the unsuitability of this model, and the intraparticle diffusion was not only the rate-controlling step [23]. The parameters of this model were calculated and presented in Table 8 [73].

It is clear that both in-particle and external mass transfer processes play an important role in adsorption kinetics. However, it is unclear which one has a greater impact on the dye absorption rate. This is solved using the Boyd curve [42]. From the equation in Table 2, the Boyd plot is obtained by plotting B_t vs. time t (Fig. 14).

Table 7
Pseudo-first- and -second-order kinetic parameters for methylene blue (MB) adsorption by perlite samples

Kinetic		P_A	P_{APTMS}	P_{MPTMS}
Models				
Pseudo-first-order	$q_{e,exp}$ (mg g^{-1})	4.6524	5.1196	5.4470
	$q_{e,cal}$ (mg g^{-1})	0.5317	2.8949	2.8988
	k_1 (min^{-1})	0.0136	0.0427	0.0242
	R^2	0.6704	0.7406	0.6286
Pseudo-second-order	$q_{e,cal}$ (mg g^{-1})	4.5526	4.9975	5.3019
	k_2 (g mg^{-1} min^{-1})	0.6075	0.7719	0.4501
	R^2	1.0000	1.0000	1.0000

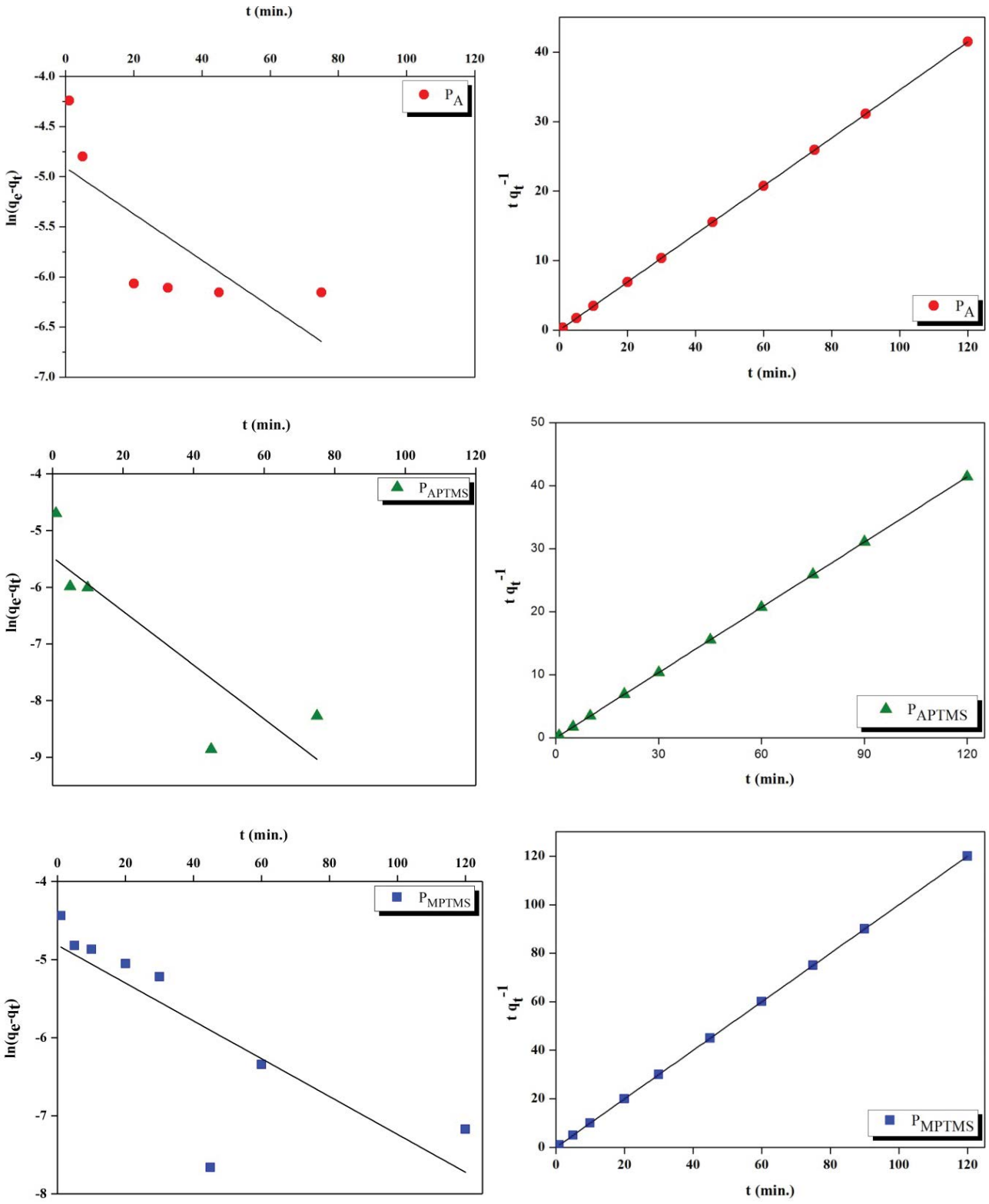

Fig. 12. Pseudo-first and second-order adsorption kinetics of MB onto P_A, P_{APTMS}, and P_{MPTMS} at 298 K.

Table 8
Parameters of intraparticle diffusion model for MB uptake by the perlites

Intraparticle						
Diffusion	P_A		P_{APTMS}		P_{MPTMS}	
Model	Value	S.E.	Value	S.E.	Value	S.E.
k_i (mg g^{-1} min$^{-1(1/2)}$)	1.48×10^{-4}	1.34×10^{-4}	1.48×10^{-4}	1.82×10^{-4}	1.32×10^{-4}	0.92×10^{-5}
C (mg g^{-1})	2.8928	9.58×10^{-4}	2.8855	5.07×10^{-4}	2.8919	5.32×10^{-4}
R^2	0.9222	–	0.9891	–	0.9993	–

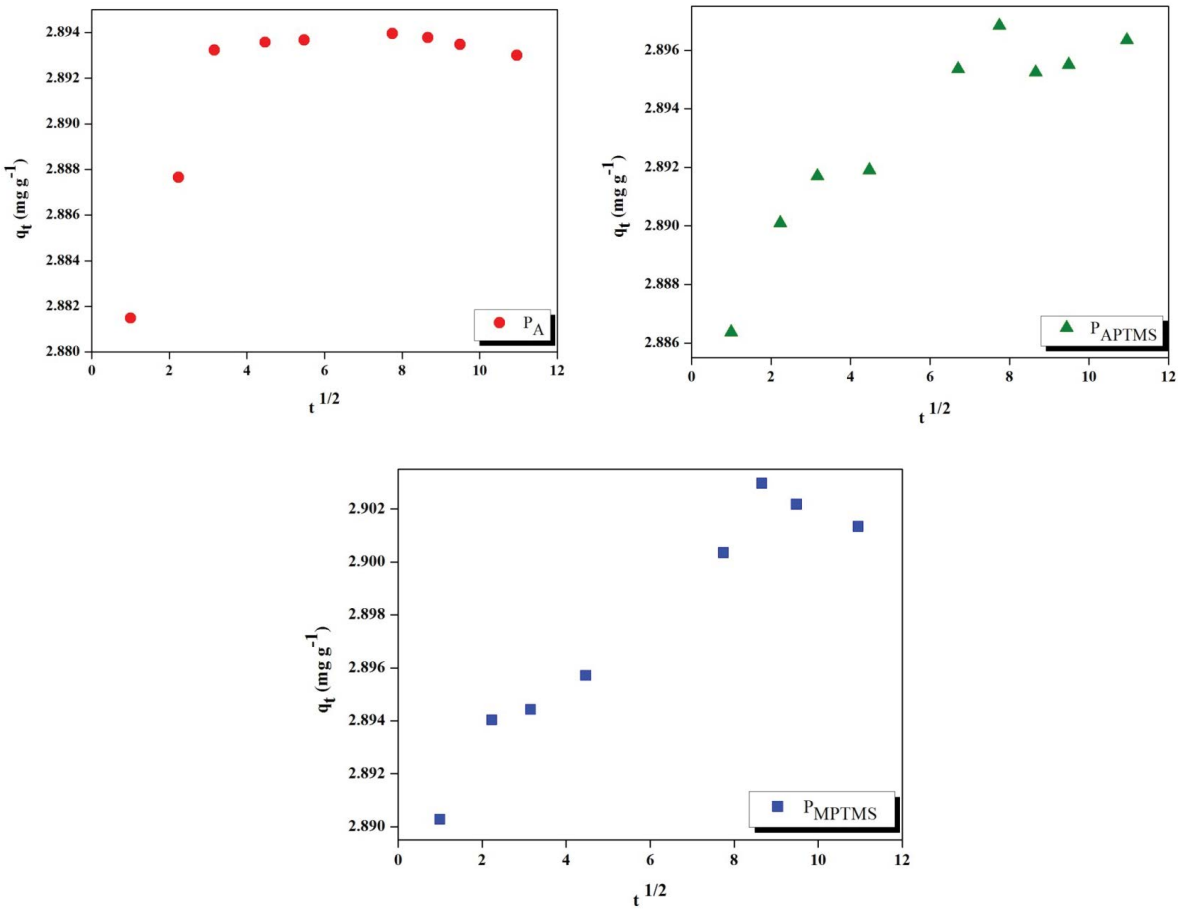

Fig. 13. Intraparticle diffusion plots for methylene blue sorption onto P_A, P_{APTMS}, and P_{MPTMS}.

If the drawn graphs are linear and pass through the origin, the pore diffusion is the slowest step. However, for all adsorbents in which MB was adsorbed, the plots of the Boyd equation are not linear and do not pass through the zero point. Therefore, film diffusion is the speed-limiting step of the adsorption process under the studied conditions [40–42,73].

3.5. Desorption of MB

A potential adsorbent used for dye removal must not only have a good adsorption capacity, but also must have an economically significant recovery capacity. HCl acid was chosen as the stripping agent for desorption processes. The selected stripping agent must be low-cost, highly efficient, and non-destructive [29,74]. Fig. 15 shows the % desorption of MB on P_A, P_{APTMS}, and P_{MPTMS} at 298 K.

As seen, the optimum desorption was achieved as 67.87% P_A, 65.64% P_{APTMS}, and 88.13% P_{MPTMS} for one cycle. The high rate of desorption of MB dye indicates that perlite and modified perlites are suitable as potential adsorbents.

3.6. Calculation analysis and proposed adsorption mechanism

In this study, quantum chemical calculations using the DFT theorem were conducted to investigate the effect of

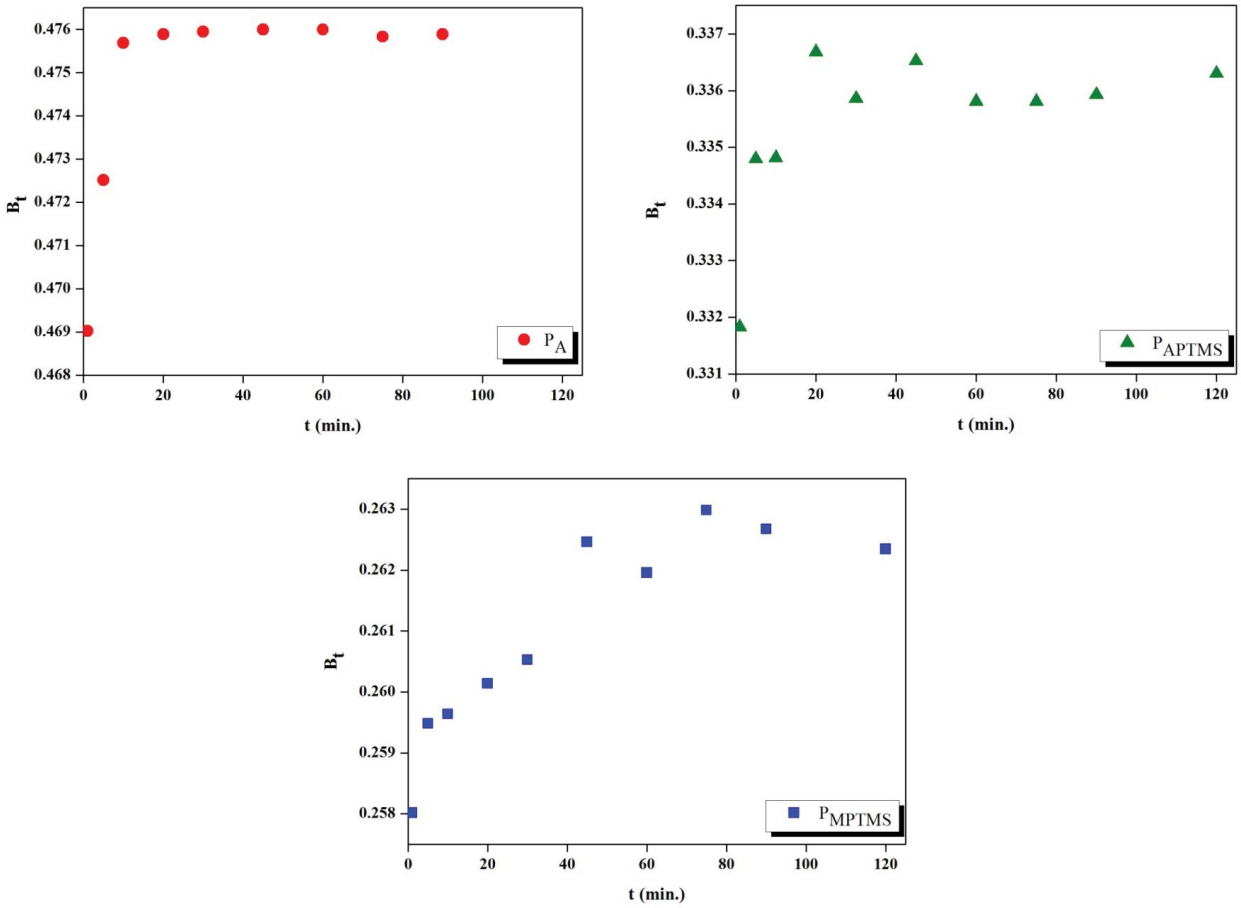

Fig. 14. Boyd plots for methylene blue sorption onto P_A, P_{APTMS}, and P_{MPTMS}.

Table 9
Calculated quantum chemical parameters of the studied molecules

Compounds	Methylene blue chloride (MB^+Cl)	(3-Mercaptopropyl) trimethoxysilane (MPTMS)	(3-Aminopropyl) trimethoxysilane (APTMS)
E_{HOMO} (eV)	–6.7804	–6.2639	–7.3987
E_{LUMO} (eV)	–0.0416	–0.4525	4.1773
Energy gap, $\Delta E = E_{LUMO} - E_{HOMO}$ (eV)	6.7388	5.8114	11.5760
Dipole moment, μ (debye)	0.2302	3.5402	1.8105
Chemical hardness, η (eV)	3.3694	2.9057	5.7880
Chemical softness, S	0.2968	0.3441	0.1728
Electronegativity, χ (eV)	3.411	3.3582	1.6107
Electrophilicity index (ω)	0.0079	0.9705	0.2832

the molecular structure on the adsorption process of MB molecules onto the P_{APTMS} and P_{MPTMS} surface. Full geometry optimizations of compounds were performed using DFT based on B3LYP and the 6–31G (d, p) orbital basis sets in Gaussian09 program [75,76]. Very useful information can be obtained by this method to examine the adsorption potentials of organic compounds. Quantum chemical parameters of compounds such as E_{HOMO}, E_{LUMO}, ΔE, μ, I, A, χ, η, w, S, ΔN, and $\Delta E_{back\ donation}$ were calculated (Table 9).

The HOMO and LUMO energy maps of MB^+Cl showed that the HOMO regions are concentrated on nitrogen and sulfur atoms. On the other hand, it is observed that the HOMO region concentrates on sulfur for MPTMS and oxygen for APTMS (Fig. 16).

The basic state geometry of the adsorbent (MB^+Cl) and adsorbed (MPTMS and APTMS) and the structure of HOMO and LUMO play a role in the activity properties. E_{HOMO} and E_{LUMO} show that the ability of the compounds to

donate and accept electrons, respectively. The energy gap (ΔE) is an important parameter as a function of the reactivity of the molecule towards adsorption on the surface. A molecule with a low ΔE is more polarized and is usually associated with high chemical activity and low kinetic stability and is called a soft molecule [77]. Dipole moment (μ_{Debye}) is another important electronic parameter. The high value of the dipole moment, probably increases the adsorption between the chemical compound and the surface [78]. Absolute hardness (η) and softness (S) are important properties used to measure the stability and reactivity of a molecule. A hard molecule has a large ΔE values, and a soft molecule has a small ΔE value [79,80]. The global electrophilicity index (ω) indicates the ability of the molecules to accept electrons [81]. Molecular electrostatic potential (MEP) provides information about reactive sites for electrophilic and nucleophilic attack as well as hydrogen-bonding interactions in molecules. The MEP was run at B3LYP/6–31G (d, p). Thus, the negative (red) regions of MEP were associated with electrophilic reactivity and nucleophilic reactivity with positive (blue) regions (Fig. 17).

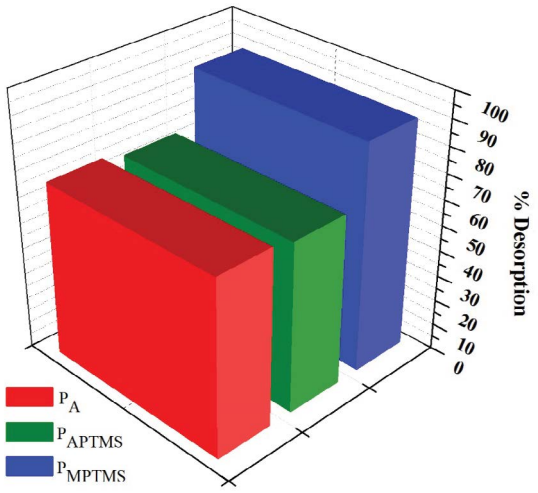

Fig. 15. Desorption (%) of MB on P_A, P_{APTMS}, and P_{MPTMS} at 298 K.

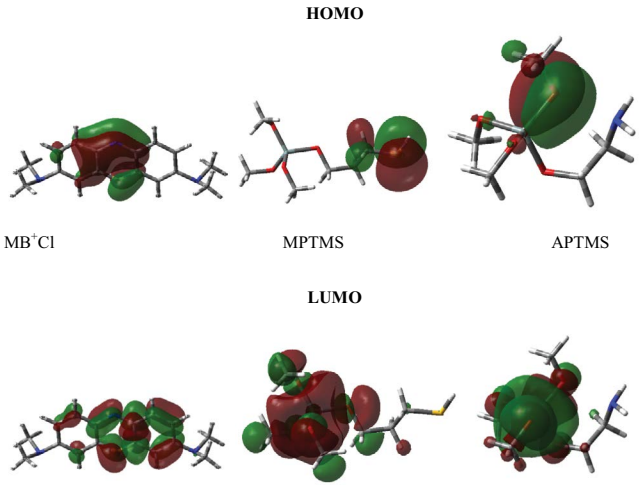

Fig. 16. HOMO and LUMO for APTMS and MPTMS.

The MB$^+$Cl, MPTMS, and APTMS may interact in two ways in solution medium according to chemical calculations data and MEPs. The solution of pH is very important for defining the reaction mechanism, so as the pollutant structure can also be differentiated according to the changes of pH (Fig. 18).

Experimental data show that electrostatic interaction is present. However, it can be said that the interaction at high pH is better.

4. Conclusions

Natural perlite was functionalized with organosilane groups, creating a more suitable adsorbent surface for dye adsorption. Impurities were removed with an HCl acid solution before modification. Experimental data were applied in linear and nonlinear Langmuir, Freundlich, Dubinin–Radushkevich (D–R), and Sips isotherm equations. The Langmuir monolayer adsorption capacities (q_m) of MB were determined to be 4.6524, 5.1196 and 5.4470 mg g^{-1} at 298 K for P_A, P_{APTMS}, and P_{MPTMS}, respectively. The adsorption of MB was found to be compatible with Freundlich isotherm model due to low S.E., χ^2, and high R^2 values. The adsorption energy (E) values obtained from the D–R adsorption isotherm are lower than 8 kJ mol^{-1}, indicating that adsorption is related to physical interactions. Physical adsorption involves electrostatic interaction and Van Der Waals bonds. The kinetic studies of MB onto P_A, P_{APTMS}, and P_{MPTMS} reveal that the adsorption behavior is better described by the PSO model than the PFO model. In addition, experiments obviously show that the adsorption of dye molecules on perlite

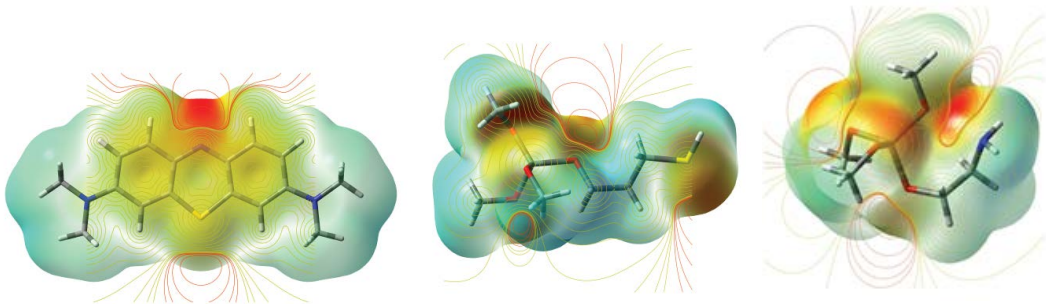

Fig. 17. MEPs for MB$^+$Cl (a), MPTMS (b), and APTMS (c).

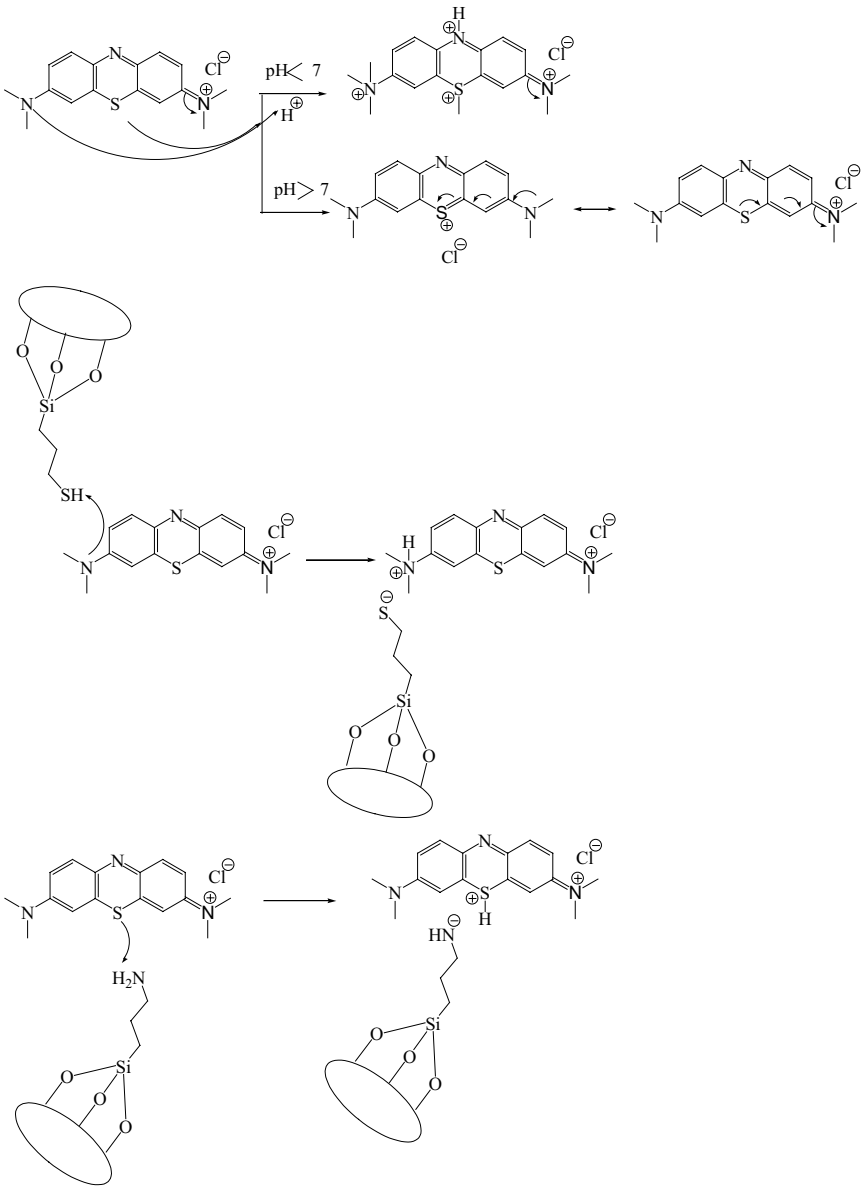

Fig. 18. pH effect and possible interactions.

samples is a multi-step process concerning transport of these molecules from the aqueous solution to the surface of the solid particles. Film diffusion is the speed-limiting step of the adsorption process under the studied conditions. According to the MEP map using the DFT/B3LYP/6–31G (d, p) base set, the negative potential region is related to electrophilic reactivity while the positive potential region is related to nucleophilic reactivity. The HOMO and LUMO energy maps of $MB^{+}Cl$ show that the HOMO region concentrates on sulfur for MPTMS and oxygen for APTMS.

Acknowledgments

Financial support was provided by the Research Fund of Yüzüncü Yıl University, Van, Turkey (Project number: FYL-2016-5291).

References

[1] É.S. Oliveira, J.M.F.d. Almeida, E. Damasceno, N.S. Fernandes, Evaluation of the applicability of thermogravimetry in the monitoring of the organofunctionalization process of expanded perlite, Thermochim. Acta, 672 (2019) 107–117.
[2] H.E. Rizk, I.M. Ahmed, S.S. Metwally, Selective sorption and separation of molybdenum ion from some fission products by impregnated perlite, Chem. Eng. Process., 124 (2018) 131–136.
[3] M. Doğan, M. Alkan, Removal of methyl violet from aqueous solution by perlite, J. Colloid Interface Sci., 267 (2003) 32–41.
[4] A. Petrella, D. Spasiano, V. Rizzi, P. Cosma, M. Race, N. De Vietro, Lead ion sorption by perlite and reuse of the exhausted material in the construction field, Appl. Sci., 8 (2018) 1882, doi: 10.3390/app8101882.
[5] M. Alkan, Ö. Demirbaş, M. Doğan, Zeta potential of unexpanded and expanded perlite samples in various electrolyte media, Microporous Mesoporous Mater., 84 (2005) 192–200.

[6] M. Doğan, M. Alkan, Y. Onganer, Adsorption of methylene blue from aqueous solution onto perlite, Water Air Soil Pollut., 120 (2000) 229–248.
[7] A. Fidalgo, L. Ilharco, Tailoring the structure and hydrophobic properties of amorphous silica by silylation, Microporous Mesoporous Mater., 158 (2012) 39–46.
[8] T. Areerob, S. Chiarakorn, N. Grisdanurak, Enhancement of gaseous BTEX adsorption on RH-MCM-41 by chlorosilanes, Sains Malaysiana, 44 (2015) 429–439.
[9] X. Liang, Y. Xu, G. Sun, L. Wang, Y. Sun, X. Qin, Preparation, characterization of thiol-functionalized silica and application for sorption of Pb^{2+} and Cd^{2+}, Colloids Surf., A, 349 (2009) 61–68.
[10] I. Kenfack, E. Ngameni, H. Tcheumi, V. Tchieda Kougoum, C. Carteret, A. Walcarius, Sorption of methylene blue on an organoclay bearing thiol groups and application to electrochemical sensing of the dye, Talanta, 74 (2008) 489–497.
[11] E. Errais, J. Duplay, F. Darragi, I. M'Rabet, A. Aubert, F. Huber, G. Morvan, Efficient anionic dye adsorption on natural untreated clay: kinetic study and thermodynamic parameters, Desalination, 275 (2011) 74–81.
[12] T. Anitha, P. Senthil Kumar, K. Sathish Kumar, Synthesis of nano-sized chitosan blended polyvinyl alcohol for the removal of Eosin Yellow dye from aqueous solution, J. Water Process. Eng., 13 (2016) 127–136.
[13] T. Tatarchuk, N. Paliychuk, R. Babu Bitra, A. Shyichuk, M. Naushad, I. Mironyuk, D. Ziolkovska, Adsorptive removal of toxic Methylene Blue and Acid Orange 7 dyes from aqueous medium using cobalt-zinc ferrite nanoadsorbents, Desal. Water Treat., 150 (2019) 374–385.
[14] W. Zhang, C. Zhou, W. Zhou, A. Lei, Q. Zhang, Q. Wan, B. Zou, Fast and considerable adsorption of methylene blue dye onto graphene oxide, Bull. Environ. Contam. Toxicol., 87 (2011) 86–90.
[15] T. Liu, Y. Li, Q. Du, J. Sun, Y. Jiao, G. Yang, Z. Wang, Y. Xia, W. Zhang, K. Wang, H. Zhu, D. Wu, Adsorption of methylene blue from aqueous solution by graphene, Colloid Surf., B, 90 (2012) 197–203.
[16] M. Naushad, A.A. Alqadami, Z.A. AlOthman, I.H. Alsohaimi, M.S. Algamdi, A.M. Aldawsari, Adsorption kinetics, isotherm and reusability studies for the removal of cationic dye from aqueous medium using arginine modified activated carbon, J. Mol. Liq., 293 (2019) 111442, doi: 10.1016/j.molliq.2019.111442.
[17] M.-X. Zhu, L. Lee, H.-H. Wang, Z. Wang, Removal of an anionic dye by adsorption/precipitation processes using alkaline white mud, J. Hazard. Mater., 149 (2007) 735–741.
[18] A. Dąbrowski, Z. Hubicki, P. Podkościelny, E. Robens, Selective removal of the heavy metal ions from waters and industrial wastewaters by ion-exchange method, Chemosphere, 56 (2004) 91–106.
[19] R. Han, J. Zhang, P. Han, Y. Wang, Z. Zhao, M. Tang, Study of equilibrium, kinetic and thermodynamic parameters about methylene blue adsorption onto natural zeolite, Chem. Eng. J., 145 (2009) 496–504.
[20] N. Zaghbani, H. Amor, M. Dhahbi, Separation of methylene blue from aqueous solution by micellar enhanced ultrafiltration, Sep. Purif. Technol., 55 (2007) 117–124.
[21] X. Chen, L. Liu, Y.Y. Peter, S.S. Mao, Increasing solar absorption for photocatalysis with black hydrogenated titanium dioxide nanocrystals, Science, 331 (2011) 746–750.
[22] M. Naushad, G. Sharma, Z.A. Alothman, Photodegradation of toxic dye using gum arabic-crosslinked-poly(acrylamide)/$Ni(OH)_2$/FeOOH nanocomposites hydrogel, J. Cleaner Prod., 241 (2019) 118263, doi: 10.1016/j.jclepro.2019.118263.
[23] E. Gokirmak Sogut, N. Caliskan, Removal of lead, copper and cadmium ions from aqueous solution using raw and thermally modified diatomite, Desal. Water Treat., 58 (2017) 154–167.
[24] S.A. Odoemelam, U.N. Emeh, N.O. Eddy, Experimental and computational chemistry studies on the removal of methylene blue and malachite green dyes from aqueous solution by neem (*Azadirachta indica*) leaves, J. Taibah Univ. Sci., 12 (2018) 255–265.
[25] K. Srithammaraj, R. Magaraphan, H. Manuspiya, Influence of thiol groups on the ethylene adsorption and conductivity properties of the modified porous clay heterostructures (PCHS) using as ethylene scavenger in smart packaging, Polym. Bull., 75 (2018) 3951–3969.
[26] P. Yuan, D. Liu, D.-Y. Tan, K.-K. Liu, H.-G. Yu, Y.-H. Zhong, A.-H. Yuan, W.-B. Yu, H.-P. He, Surface silylation of mesoporous/macroporous diatomite (diatomaceous earth) and its function in Cu(II) adsorption: the effects of heating pretreatment, Microporous Mesoporous Mater., 170 (2013) 9–19.
[27] M. Ertaş, B. Acemioğlu, M.H. Alma, M. Usta, Removal of methylene blue from aqueous solution using cotton stalk, cotton waste and cotton dust, J. Hazard. Mater., 183 (2010) 421–427.
[28] N. Fiol, I. Villaescusa, Determination of sorbent point zero charge: usefulness in sorption studies, Environ. Chem. Lett., 7 (2009) 79–84.
[29] H. El Boujaady, M. Mourabet, M. Bennani-Ziatni, A. Taitai, Adsorption/desorption of Direct Yellow 28 on apatitic phosphate: mechanism, kinetic and thermodynamic studies, J. Assoc. Arab. Univ. Basic Appl. Sci., 16 (2014) 64–73.
[30] N. Çalışkan Kılıç, E. Gökırmak Söğüt, A. Savran, A. Kul, Ş. Kubilay, Removal of Cu(II) and Cd(II) ions from aqueous solutions using local raw material as adsorbent: a study in binary systems, Desal. Water Treat., 72 (2017) 1–16.
[31] M. Rahman, K. Sathasivam, Heavy metal adsorption onto *Kappaphycus* sp. from aqueous solutions: the use of error functions for validation of isotherm and kinetics models, Biomed. Res. Int., 2015 (2015) 126298, doi: 10.1155/2015/126298.
[32] M.R. Samarghandi, M. Hadi, S. Moayedi, F. Askari, Two-parameter isotherms of methyl orange sorption by pinecone derived activated carbon, J. Environ. Health Sci., 6 (2009) 285–294.
[33] S.-C. Tsai, K.-W. Juang, Comparison of linear and non-linear forms of isotherm models for strontium sorption on a sodium bentonite, J. Radioanal. Nucl. Chem., 243 (2000) 741–746.
[34] N. Caliskan, A.R. Kul, S. Alkan, E.G. Sogut, İ. Alacabey, Adsorption of Zinc(II) on diatomite and manganese-oxide-modified diatomite: a kinetic and equilibrium study, J. Hazard. Mater., 193 (2011) 27–36.
[35] X. Chen, Modeling of experimental adsorption isotherm data, Information, 6 (2015) 14–22.
[36] C. Nguyen, D.D. Do, The Dubinin–Radushkevich equation and the underlying microscopic adsorption description, Carbon, 39 (2001) 1327–1336.
[37] R. Thotagamuge, N. Hamdan, M. Petra, K. Tennakoon, P. Ekanayake, Equilibrium isotherm studies of adsorption of pigments extracted from Kuduk-kuduk (*Melastoma malabathricum* L.) pulp onto TiO_2 nanoparticles, J. Chem., 2014 (2014) 1–6 p.
[38] Y.C. Wong, Y.S. Szeto, W.H. Cheung, G. McKay, Equilibrium studies for acid dye adsorption onto chitosan, Langmuir, 19 (2003) 7888–7894.
[39] E. Gökırmak Söğüt, N. Caliskan, Isotherm and kinetic studies of Pb(II) adsorption on raw and modified diatomite by using non-linear regression method, Fresenius Environ. Bull., 26 (2017).
[40] N. Suriyanon, P. Punyapalakul, C. Ngamcharussrivichai, Mechanistic study of diclofenac and carbamazepine adsorption on functionalized silica-based porous materials, Chem. Eng. J., 214 (2013) 208–218.
[41] K.V. Kumar, V. Ramamurthi, S. Sivanesan, Modeling the mechanism involved during the sorption of methylene blue onto fly ash, J. Colloid Interface Sci., 284 (2005) 14–21.
[42] D. Kumar, J.P. Gaur, Chemical reaction- and particle diffusion-based kinetic modeling of metal biosorption by a *Phormidium* sp.-dominated cyanobacterial mat, Bioresour. Technol., 102 (2011) 633–640.
[43] E. Ergan, E. Akbas, Studies on theoretical calculations of corrosion inhibition behavior of pyridazine and pyrazole derivatives, Fresenius Environ. Bull., 27 (2018) 9549–9556.
[44] S. Shahabi, P. Norouzi, M.R. Ganjali, Theoretical and electrochemical study of carbon steel corrosion inhibition in the presence of two synthesized schiff base inhibitors: application of fast Fourier transform continuous cyclic voltammetry to study the adsorption behavior, Int. J. Electrochem. Sci., 10 (2015) 2646–2662.

[45] R.G. Parr, L.V. Szentpály, S. Liu, Electrophilicity index, J. Am. Chem. Soc., 121 (1999) 1922–1924.
[46] P.K. Chattaraj, D.R. Roy, Update 1 of: electrophilicity index, Chem. Rev., 107 (2007) PR46–PR74.
[47] Y. Karzazi, M. McHarfi, A. Dafali, B. Hammouti, A theoretical investigation on the corrosion inhibition of mild steel by piperidine derivatives in hydrochloric acid solution, J. Chem. Pharm., 6 (2014) 689–696.
[48] M.A. Moreira, K.J. Ciuffi, V. Rives, M.A. Vicente, R. Trujillano, A. Gil, S.A. Korili, E.H. de Faria, Effect of chemical modification of palygorskite and sepiolite by 3-aminopropyltriethoxisilane on adsorption of cationic and anionic dyes, Appl. Clay Sci., 135 (2017) 394–404.
[49] A. Celik, A. Kilic, G. Çakal, Expanded perlite aggregate characterization for use as a lightweight construction raw material, Physicochem. Probl. Miner. Process., 49 (2013) 689–700.
[50] J. Rodriguez, F. Soria, H. Geronazzo, H. Destefanis, Modification and characterization of natural aluminosilicates, expanded perlite, and its application to immobilise α – amylase from *A. oryzae*, J. Mol. Catal. B: Enzym., 133 (2016) S259–S270.
[51] A. de Mello Ferreira Guimarães, V.S.T. Ciminelli, W.L. Vasconcelos, Smectite organofunctionalized with thiol groups for adsorption of heavy metal ions, Appl. Clay Sci., 42 (2009) 410–414.
[52] Z. Zujovic, W. Wheelwright, P. Kilmartin, J. Hanna, R. Cooney, Structural investigations of perlite and expanded perlite using 1 H, 27 Al and 29 Si solid-state NMR, Ceram. Int., 44 (2017) 2952–2958, doi: 10.1016/j.ceramint.2017.11.047.
[53] P. Li, L.M. Ng, Surface chemistry of alkyl and perfluoro ethers: a FTIR study of adsorption and thermal desorption of $(C_2H_3)_2O$ and $(C_2F_5)_2O$ on SiO_2, Surf. Sci., 342 (1995) 359–369.
[54] Z. Xia, L. Baird, N. Zimmerman, M. Yeager, Heavy metal ion removal by thiol functionalized aluminum oxide hydroxide nanowhiskers, Appl. Surf. Sci., 416 (2017) 565–573.
[55] S. Kabra, S. Katara, A. Rani, Characterization and study of Turkish perlite, Int. J. Innovative Res. Sci. Eng. Technol., 3297 (2007) 4320–4326.
[56] T.S. Anirudhan, R. Chandran, Adsorptive removal of basic dyes from aqueous solutions by surfactant modified bentonite clay (organoclay): kinetic and competitive adsorption isotherm, Process Saf. Environ. Prot., 95 (2015) 215–225.
[57] M. Roulia, A.A. Vassiliadis, Sorption characterization of a cationic dye retained by clays and perlite, Microporous Mesoporous Mater., 116 (2008) 732–740.
[58] I. Ruggiero, M. Terracciano, N.M. Martucci, L. De Stefano, N. Migliaccio, R. Tatè, I. Rendina, P. Arcari, A. Lamberti, I. Rea, Diatomite silica nanoparticles for drug delivery, Nanoscale Res. Lett., 9 (2014) 329, doi: 10.1186/1556-276X-9-329.
[59] M. Doğan, M. Alkan, Ü. Çakir, Electrokinetic properties of perlite, J. Colloid Interface Sci., 192 (1997) 114–118.
[60] M. Alkan, G. Dolu, H. Namli, Zeta potentials of perlite modified with dimethyl-dichlorosilane, 3-aminopropyltriethoxysilane and dimethyloctadecylchlorosilane, Fresenius Environ. Bull., 14 (2005) 795–802.
[61] J.U.K. Oubagaranadin, N. Sathyamurthy, Z.V.P. Murthy, Evaluation of Fuller's earth for the adsorption of mercury from aqueous solutions: a comparative study with activated carbon, J. Hazard. Mater., 142 (2007) 165–174.
[62] D. Pathania, S. Sharma, P. Singh, Removal of methylene blue by adsorption onto activated carbon developed from *Ficus carica* bast, Arabian J. Chem., 10 (2017) S1445–S1451.
[63] Ş. Parlayici, Alginate-coated perlite beads for the efficient removal of methylene blue, malachite green, and methyl violet from aqueous solutions: kinetic, thermodynamic, and equilibrium studies, J. Anal. Sci. Technol., 10 (2019) 4, doi: 10.1186/s40543–019–0165–5.
[64] Z. Derakhshan, M. Baghapour, M. Ranjbar, M. Faramarzian, Adsorption of methylene blue dye from aqueous solutions by modified pumice stone: kinetics and equilibrium studies, Health Scope, 2 (2013) 136–144.
[65] M. Ge, L. Cao, M. Du, G. Hu, S.M. Jahangir Alam, Competitive adsorption analyses of a pure magadiite and a new silylated magadiite on methylene blue and phenol from related aqueous solution, Mater. Chem. Phys., 217 (2018) 393–402.
[66] D. Chen, H. Zhang, K. Yang, H. Wang, Functionalization of 4-aminothiophenol and 3-aminopropyltriethoxysilane with graphene oxide for potential dye and copper removal, J. Hazard. Mater., 310 (2016) 179–187.
[67] H.A. Al-Aoh, R. Yahya, M. Jamil Maah, M. Radzi Bin Abas, Adsorption of methylene blue on activated carbon fiber prepared from coconut husk: isotherm, kinetics and thermodynamics studies, Desal. Water Treat., 52 (2014) 6720–6732.
[68] A.-A.A. Omar, A.H. Yahaya, R. Yahya, H.A. Al-Aoh, isotherm parameters of methylene blue adsorption on coconut husk fiber based-activated carbon, World Appl. Sci. J., 31 (2014) 1–4.
[69] H.A. Al-Aoh, I.A.M. Mihaina, M.A. Alsharif, A.A.A. Darwish, M. Rashad, S.K. Mustafa, M.M.H. Aljohani, M.A. Al-Duais, H.S. Al-Shehri, Removal of methylene blue from synthetic wastewater by the selected metallic oxides nanoparticles adsorbent: equilibrium, kinetic and thermodynamic studies, Chem. Commun., 207 (2020) 1719–1735.
[70] W. Syie Luing, N. Ngadi, I. Inuwa, O. Hassan, Recent advances in applications of activated carbon from biowaste for wastewater treatment: a short review, J. Cleaner Prod., 175 (2018) 361–375.
[71] Z.-H. Yu, S.-R. Zhai, H. Guo, T.-M. lv, Y. Song, F. Zhang, H.-C. Ma, Removal of methylene blue over low-cost mesoporous silica nanoparticles prepared with naturally occurring diatomite, J. Sol-Gel Sci. Technol., 88 (2018) 541–550.
[72] P. Demirçivi, Synthesis and characterization of Zr(IV) doped immobilized cross-linked chitosan/perlite composite for acid orange II adsorption, Int. J. Biol. Macromol., 118 (2018) 340–346.
[73] E.A. Mohamed, A.Q. Selim, A.M. Zayed, S. Komarneni, M. Mobarak, M.K. Seliem, Enhancing adsorption capacity of Egyptian diatomaceous earth by thermo-chemical purification: methylene blue uptake, J. Colloid Interface Sci., 534 (2019) 408–419.
[74] K.G. Akpomie, F.A. Dawodu, K.O. Adebowale, Mechanism on the sorption of heavy metals from binary-solution by a low cost montmorillonite and its desorption potential, Alex. Eng. J., 54 (2015) 757–767.
[75] C. Lee, W. Yang, R.G. Parr, Development of the Colle-Salvetti correlation-energy formula into a functional of the electron density, Phys. Rev. B, 37 (1988) 785–789.
[76] M. ElBelghiti, Y. Karzazi, A. Dafali, B. Hammouti, F. Bentiss, I.B. Obot, I. Bahadur, E.E. Ebenso, Experimental, quantum chemical and Monte Carlo simulation studies of 3,5-disubstituted-4-amino-1,2,4-triazoles as corrosion inhibitors on mild steel in acidic medium, J. Mol. Liq., 218 (2016) 281–293.
[77] I. Fleming, Frontier Orbitals and Organic Chemical Reactions, Wiley, London; New York, NY, 1976.
[78] X. Li, S. Deng, H. Fu, T. Li, Adsorption and inhibition effect of 6-benzylaminopurine on cold rolled steel in 1.0M HCl, Electrochim. Acta, 54 (2009) 4089–4098.
[79] N. Obi-Egbedi, I. Obot, M. El-Khaiary, S. Umoren, E. Ebenso, Computational simulation and statistical analysis on the relationship between corrosion inhibition efficiency and molecular structure of some phenanthroline derivatives on mild steel surface, Int. J. Electrochem. Sci., 6 (2011) 5649–5675.
[80] R. Hasanov, M. Sadıkoğlu, S. Bilgiç, Electrochemical and quantum chemical studies of some Schiff bases on the corrosion of steel in H_2SO_4 solution, Appl. Surf. Sci., 253 (2007) 3913–3921.
[81] P. Udhayakala, T.V. Rajendiran, S. Gunasekaran, Theoretical evaluation of corrosion inhibition performance of some triazole derivatives, J. Adv. Sci. Res., 3 (2012) 71–77.